**Title**
Parametric Amplification with Surface Acoustic Waves



**Author**
Lu, Ting

**Publication Date**
2018

Peer reviewed|Thesis/dissertation

UNIVERSITY OF CALIFORNIA

Los Angeles

# Parametric Amplification with Surface Acoustic Waves

A thesis submitted in partial satisfaction

of the requirements for the degree Master of Science

in Electrical and Computer Engineering

by

Ting Lu

2018

ABSTRACT OF THE THESIS

Parametric Amplification with Surface Acoustic Waves

by

Ting Lu

Master of Science in Electrical and Computer Engineering

University of California, Los Angeles, 2018

Professor Yuanxun Wang, Chair

This work is to explore the time-reversal symmetry breaking employing an acoustic wave platform through space-time parametric modulations, for the purpose of developing nonlinear devices such as amplifiers and mixers. The strength of acoustic wave platform is that it can obtain great leverage on the slow velocity and small wavelength of acoustic waves at RF to minimize the footprint of transmission lines. To realize parametric amplification, nonlinear Surface Acoustic Wave(SAW) grating is employed to pump a dynamic biasing electric field into the piezoelectric material to couple the pump electromagnetic wave to the propagating surface acoustic waves in the condition of phase matched. Two different ways to achieve nonlinear change of piezoelectric coefficient and elastic stiffness are proposed: 1) Material nonlinearity using ferromagnetic material like BST; 2) Geometrical nonlinearity using the coupling between vertical and parallel stiffness. The fractional modulation of elastic stiffness is approximate 4% in the first approach and can reach 10% or even higher in the second approach. Simulation validation using COMSOL demonstrates the parametric fixing effects produced on the Surface Acoustic Wave devices. Fabrication and characterization of Surface Acoustic Wave delay lines are also provided.

The thesis of Ting Lu is approved.

Tatsuo Itoh

Gregory P. Carman

Yuanxun Wang, Committee Chair

University of California, Los Angeles

2018

# TABLE OF CONTENTS

# LIST OF FIGURES

# ACKNOWLEDGMENTS

I would like to express my gratitude to my advisor, Professor Yuanxun Wang, for his professional comments, remarks, and engagement throughout this work. Professor Wang is always willing to help when I run into puzzles of my research. I would also like to thank Professor Tatsuo Itoh and Professor Greg Carman for reviewing and providing help for this thesis. It's a great honor for me to have them serve as my committee members. In addition, I would like to thank Joseph Schneider for the help in fabricating Surface Acoustic Wave Device, also thank Zhi Yao for helpful discussions with me regarding this work. Finally, I would like to thank the Emerging Frontiers in Research and Innovation (EFRI) program of National Science Foundation for financial support.

# CHAPTER 1

# Introduction

Non-reciprocal devices are key components in the wireless industry. However, the application of traditional non-reciprocal devices is impeded by their bulky size and poor performance. Here, our work is to explore non-reciprocal concepts on acoustic wave platform using parametric amplification, with the aim to develop a new class of non-reciprocal acoustic components such as acoustic circulators, and nonlinear devices such as mixers and amplifiers, which can provide orders of magnitude improvement in dramatically reduces sizes.

## 1.1 Background and Motivation

The wireless industry has changed our lives in many different ways in the past decade. This change is largely attributed to the semiconductor advancement based integrated circuit(IC) technology which generates fasted, smaller and more power efficient mobile devices. However, some limitations of the IC technology such as inability to produce non-reciprocity and high quality factors in on-chip passive components still remain and need further resolving.

Traditional non-reciprocal devices, usually made of ferrite magnetic materials are very bulky, narrow band and difficult to tune. What's more, ferrites cannot be integrated on the semiconductor-based IC using standard manufacturing process. To solve this problem, a UCLA group proposed a time-varying transmission line(TVTL) [1] to separate the overlapping signals in time, frequency and space to resolve this issue. When the signal wave propagates in the same direction of the pump wave on the time-varying transmission line, it will mix and get amplified by the pump wave. The signal wave that propagates in the opposite direction of the pump wave will not mix with it. Consequently, the difference in the propagation direction will result in difference of the signal frequencies, which can be used in the non-reciprocal devices.

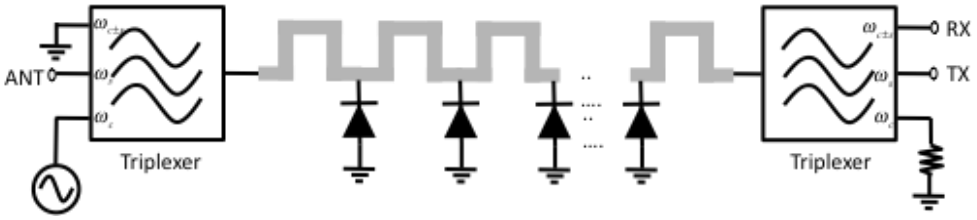


(a)

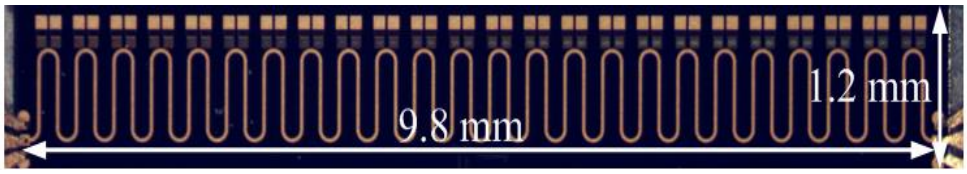


(b)

Figure 1.1.1: (a) Schematic of On-chip circulation based on TVTL (b) Picture of TVTL chip

Based on these concepts, a circulator design [2] was demonstrated on GaN IC by the same group in UCLA, which achieve greater than 25dB isolation from 600MHz to 1.5GHz with the insertion loss less than 1.5dB for the balanced GaN DMC MMIC circulator. A frequency translational RF receiver [3] and Sequentially-Switched Delay Line (SSDL) [4] based on time varying transmission line(TVTL) also obtain superior return loss and isolation, which demonstrates the great potential of time varying transmission line (TVTL) to be applied in commercial products in markets.

To further shrink the device size but remain desirable non-reciprocal characteristics, we propose to explore the time varying transmission line concepts on the surface acoustic wave platform which has the strength of slow velocity and short wavelength at RF, based on the analogy between electromagnetic wave and surface acoustic wave.

## 1.2 Recent Developments on Non-reciprocal SAW device

Similar symmetry breaking concepts through time modulations were proposed and implemented in many other platforms, for example, in photonics [5] and acoustics [6]. Surface acoustic wave devices have been widely used as delay lines and filters with excellent quality factors and low losses. Many researches aiming at combining the concept of non-reciprocity with the well-developed surface acoustic wave field has already been conducted, with the coupling happening

using external varactor circuits [7], magnetic materials [8] or semiconductors [9]. However, they all have limitations that will impede their applications.

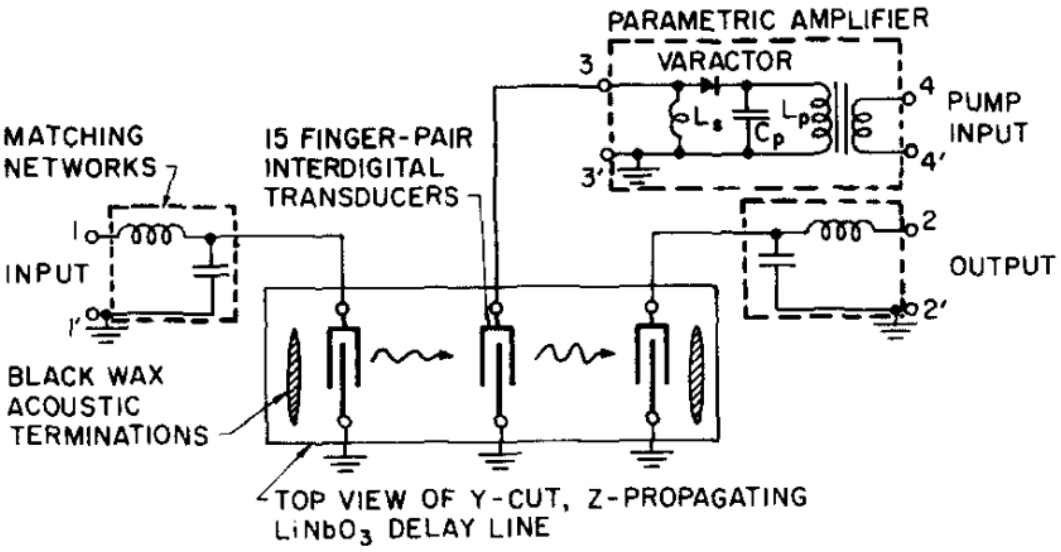


Figure 1.2.1: Schematic of surface acoustic wave amplifier

Parametric surface acoustic wave amplifier can be realized using lumped-element varactor parametric amplifier attached to the electrical port of an interdigital surface acoustic wave transducer as shown in Figure 1.2.1. [7] Terminal gain of 1~2 dB was observed in the forward direction. The isolation between forward direction and backward direction is about 5dB. However, passive loading of the center transducer by the parametric circuit brings relatively high insertion loss, and the chip size remains large due to the varactor circuits.

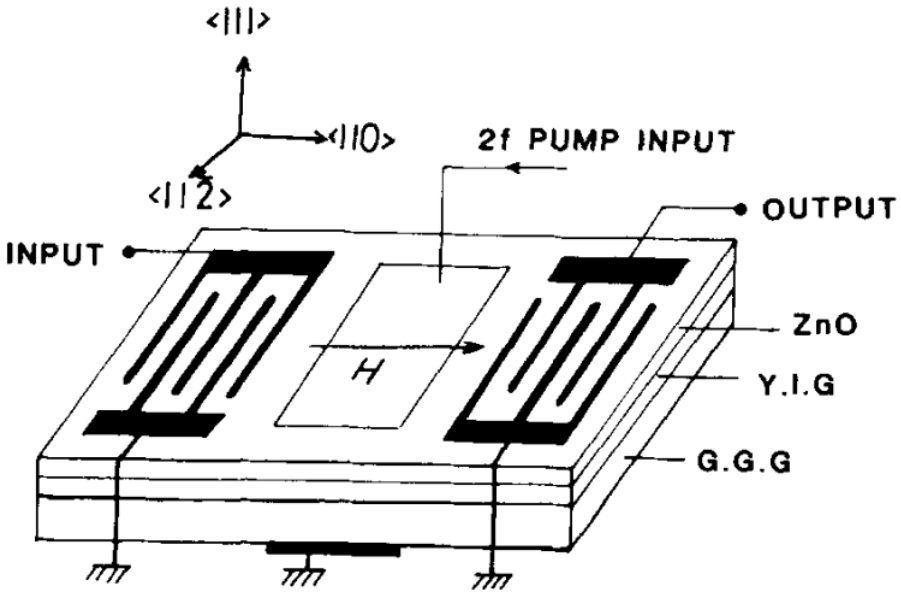


Figure 1.2.2: Schematic of ZnO-Ga doped yttrium iron garnet (YIG) and GGG structure

Interactions of surface acoustic wave with magnetization are investigated on a ZnO-Ga doped yttrium iron garnet (YIG) and GGG structure [8]. Nonlinear interaction between surface acoustic wave and magnetization contributes to the parametric effect on the acoustic wave. Parametric amplification of SAW is closely related to the magnetic field strength and input power. The amplification gain is 5.1dB at the optimum magnetic field and input power. However, the coupling between magnetization and acoustic wave will induce the energy change from surface wave to leaky bulk wave, thus increase the loss in the device.

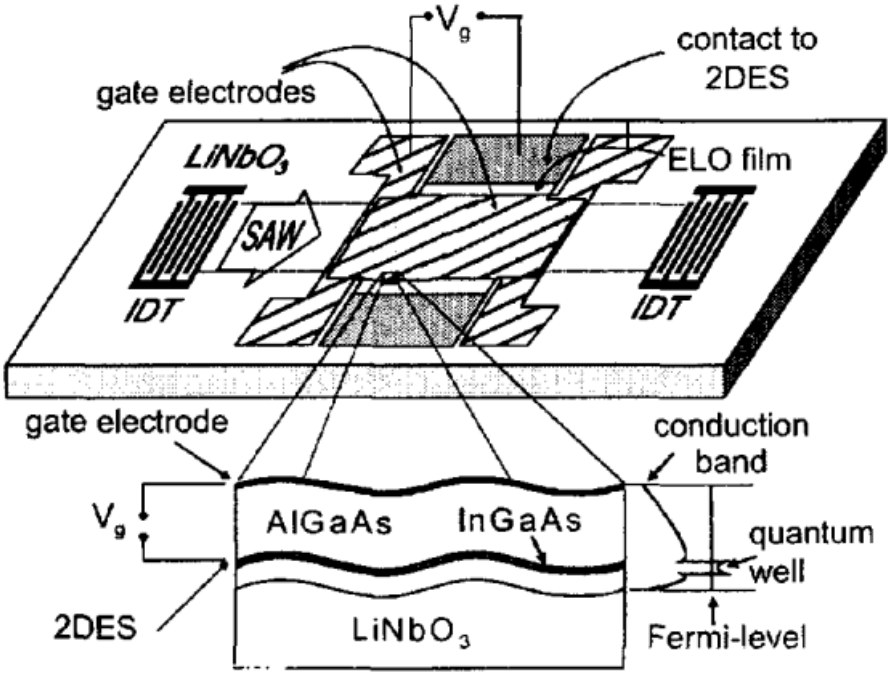


Figure 1.2.3: Schematic of piezoelectric substrate and semiconductor heterojunction

The combination of high mobility of semiconductor heterojunction and strongly piezoelectric crystals provides promising hybrids for non-reciprocal devices with surface acoustic wave [9]. The nonlinear interaction between surface acoustic wave on Lithium Niobate substrate and the free carriers in a semiconductor quantum wall results in 13.2dB isolation of opposite SAW propagation. However, the noise in the device is larger than that of passive devices because the introduction of electrons brings in noise.

## 1.3 New idea: Nonlinear SAW grating

Based on the limitations of current non-reciprocal Surface Acoustic Wave devices, we propose to explore the parametric amplification concept on the acoustic wave platform, by employing a nonlinear Surface Acoustic Wave grating to couple the energy between electromagnetic wave and acoustic wave. Analysis shows the nonlinearity can be achieved by either material properties or periodic structures, which can be used to couple the pump wave to the signal wave. Simulation

validation using COMSOL demonstrates the parametric fixing effects produced on the Surface Acoustic Wave devices using the proposed approach. Fabrication and characterization of Surface Acoustic Wave delay lines are also provided, and future works are listed.

# CHAPTER 2

# Parametric Amplification on Surface Acoustic Wave

In this chapter, we first introduce the theory of time varying transmission line [1], then demonstrate our proposed structure to implement the parametric amplification on the surface acoustic wave platform. Nonlinearity is required for modulating the mechanical stiffness by electric field. Our analysis shows 4% change of stiffness can be obtained by some ferroelectric material, and 10% change of stiffness or even higher can be realized by certain structures.

## 2.1 Time Varying Transmission Line (TVTL)

The theory of Time Varying Transmission Line can be briefly summarized as follows. To realize time varying transmission line [1], a nonlinear transmission line whose material property is modulated by the amplitude of the wave is used. A signal wave and a modulation wave are both launched into the same nonlinear transmission line propagating toward the +z direction at the angular frequencies $\omega_s$ and $\omega_m$ respectively. The modulation frequency is normally chosen to be greater than the signal frequency ($\omega_m > \omega_s$) in order to realize gains. Because of the nonlinearity of the material property such as the capacitance of the transmission line, the signal wave is mixed with the modulation wave, generating two sidebands of the carrier, $\omega_{m-s} = \omega_m - \omega_s$ and $\omega_{m+s} = \omega_m + \omega_s$. Assume the variation of the capacitance is small and transmission line is non-dispersive over the bandwidth interested, the phase matching condition can be written as:

$$\frac{\omega_s}{\beta_s} = \frac{\omega_{m-s}}{\beta_{m-s}} = \frac{\omega_{m+s}}{\beta_{m+s}} = \frac{\omega_m}{\beta_m} = v_p = \frac{1}{\sqrt{L'C_0'}} \tag{2.1.1}$$

The boundary condition at the source is:

$$v(0,t) = V_0 \cos(\omega_s t + \phi_s) \tag{2.1.2}$$

Using the boundary condition, a solution for the voltage along TVTL can be derived as follows:

$$v(z,t) = V_s(z)\cos(\omega_s t - \beta_s z + \phi_s) + V_{m-s}(z)\cos(\omega_{m-s} t - \beta_{m-s} z + \phi_m - \phi_s) +$$

$$V_{m+s}(z)\cos(\omega_{m+s} t - \beta_{m+s} z + \phi_m + \phi_s) \quad (2.1.3)$$

The amplitude of these three voltages in Equation (1.1.3) are functions of the propagation distance expressed as the following:

$$V_s(z) = V_0 \cos(\frac{1}{2\sqrt{2}} \xi \beta_s z) \quad (2.1.4.1)$$

$$V_{m-s}(z) = -\frac{V_0}{\sqrt{2}} \frac{\beta_{m-s}}{\beta_s} \sin(\frac{1}{2\sqrt{2}} \xi \beta_s z) \quad (2.1.4.2)$$

$$V_{m+s}(z) = -\frac{V_0}{\sqrt{2}} \frac{\beta_{m+s}}{\beta_s} \sin(\frac{1}{2\sqrt{2}} \xi \beta_s z) \quad (2.1.4.3)$$

where $\xi = C'_m / C'_0$ is defined as the capacitance modulation index. As shown in the results, if $\beta_{m-s}$, $\beta_s$, $\beta_{m+s}$ and z are carefully chosen, the magnitude of up converted wave and down converted wave can be larger than that of original wave. In other words, gain can be realized using time-varying transmission line.

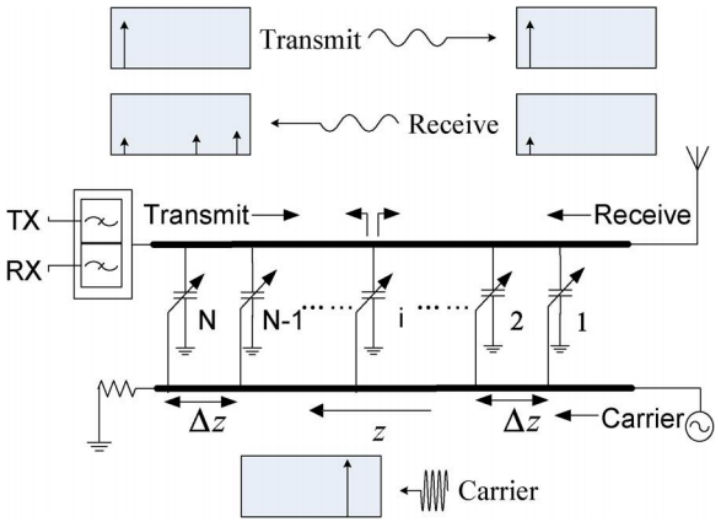


Figure 2.1.1: Schematic of Time Varying Transmission Line

On the contrast, if the signal wave travels in the opposite direction to that of the carrier wave, no solution can be obtained, which implies that no energy is coupled between the signal wave and the waves at the sidebands. The directional dependency of the parametric conversion, as a unique property of time varying transmission line, can be utilized to develop non-reciprocal components

at RF front ends. The waves which travels in different directions of the time varying transmission line will result in different frequencies at the two ends of the transmission line, with one coupling to the up converted and down converted frequency while the other remaining the same. The resulting non-reciprocity is intrinsically broadband, because it is not based on resonance structures like a conventional ferrite circulator. Because the time varying transmission line has only reactance-based components, it has very low loss and low noise characteristics. Combining with the solution of time varying transmission line provided in the previous equation, not only gain but also non-reciprocity can be obtained using time varying transmission line, which demonstrates its application in the RF front ends.

## 2.2 Nonlinear SAW Grating

Surface acoustic wave is analogous to electromagnetic wave, and we can expect similar parametric mixing and amplification effects existed in surface acoustic wave. The strength of acoustic wave is that it has small wavelength at RF frequency, therefore the surface acoustic wave device that can realize parametric amplification will have much smaller size than electrical counterpart.
In this work, we focus on parametric modulation of acoustic wave using electric field dependent stiffness to couple the energy from electromagnetic wave to propagating acoustic wave. The nonlinear stiffness can be obtained by either material nonlinearity or structure nonlinearity, which will be demonstrated in the following sections. The mechanical stiffness can be tuned by 4% using the nonlinearity of material, and it can be tuned by 10% or even higher using the nonlinearity created by structure.

The layout for surface acoustic wave parametric modulation grating is shown in Fig. 2.2.1(a). Here, we use the distributed parametric modulation grating structure to sum the nonlinearity up and create a larger output. The uni-directional Interdigital transducer (IDT) is used to guide surface acoustic wave in the desired direction without energy propagation in the undesired direction, therefore it can feed the strong electric field of the pumping wave into the grating very efficiently. To meet the phase matching requirement for parametric modulation,

phase delay is created using one 90 degree phase shifter, so that the grating will create elastic stiffness modulation as a travelling wave with phase match to any propagating acoustic wave in the same propagation direction. And the spacing and dimension of the IDT is specially designed to generate the travelling phase of stiffness modulation.

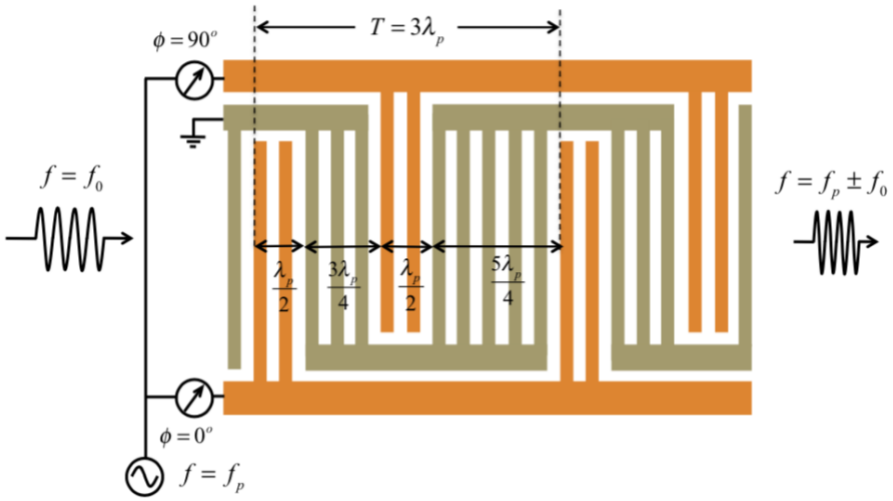


(a)

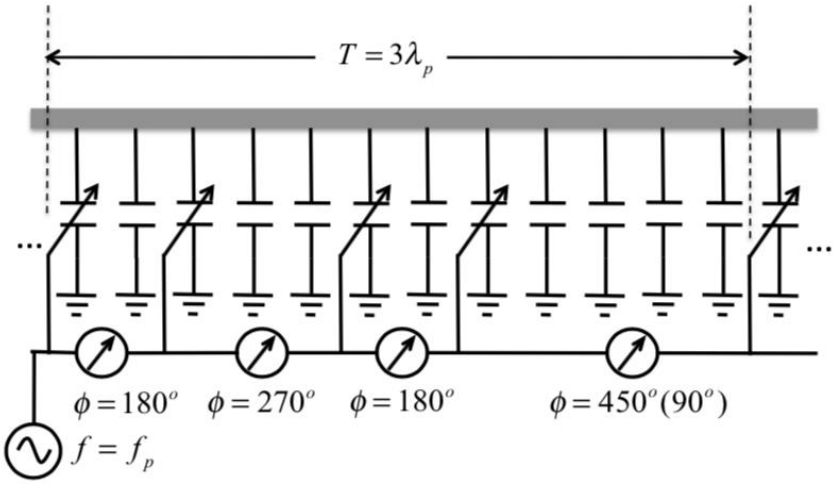


(b)

Figure 2.2.1: (a)Layout of the parametric modulation grating in the form of uni-directional IDT at the pump wave (b)Equivalent transmission line circuit

Equivalent transmission line circuit is of the parametric modulation grating is shown in Fig. 2.2.1(b). Electrical field dependent stiffness in the nonlinear surface acoustic wave grating is analogous to the voltage dependent varactors in the time varying transmission line. The varactor in the equivalent transmission line circuit represents the gap between the ground electrode and signal electrode in the layout of parametric modulation surface acoustic wave grating. Correspondingly, the capacitor in the equivalent transmission line circuit represents the gap between the ground electrodes or between the signal electrodes with same excitation. In this way, we can implement parametric amplification on the surface acoustic wave platform in an energy-efficient and size-reduced way.

## 2.3 Material Nonlinearity

We have two ways to create nonlinearity in the surface acoustic wave platform. First way to create nonlinear in piezoelectric material is to use the intrinsic property of the material itself. Although most piezoelectric material is strict linear, including the lithium Niobate ($LiNbO_3$) which is used often in surface acoustic wave device, some ferroelectric materials like Barium Strontium Titanite (BST) that is specially designed for tuning applications have 4% tunability of mechanical stiffness.

Barium Strontium Titanite, as a piezoelectric material famous for its tunable permittivity, has been largely used in making varactors [10] and tunable thin film Bulk Acoustic Wave Resonator [11]. The tunability of permittivity with applied dc voltage is shown in Fig.2.3.1. The change of permittivity can be coupled to mechanical stiffness, which can be used in our structures for parametric amplification application. The change of mechanical stiffness can be demonstrated and calculated by nonlinear coupling constitute equation. [12]

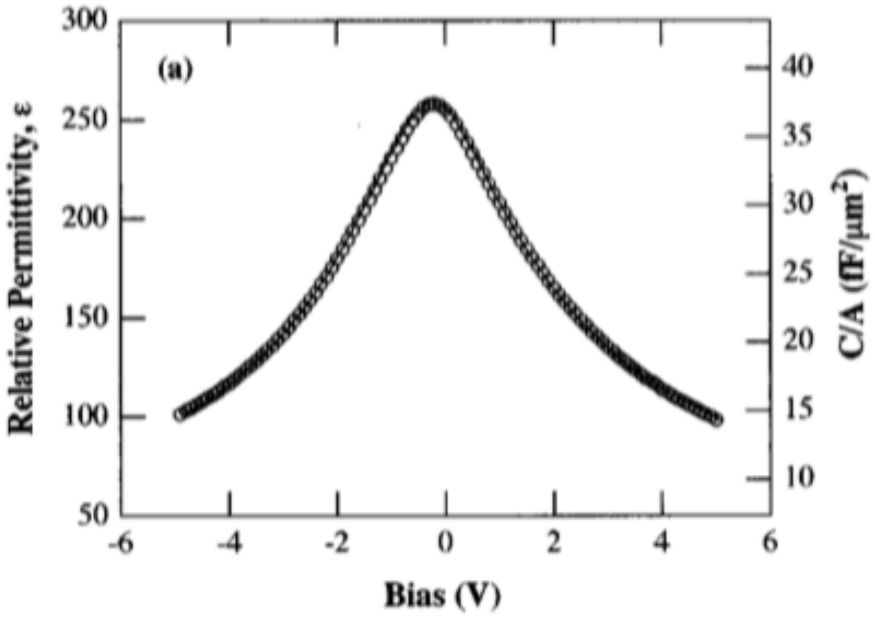


Figure 2.3.1 relative permittivity as a function of applied dc voltage

The derivation of nonlinear constitutive equation begins with Landau Theory Polarization Expansion appended with elastic energy and the energy of electrometrical coupling:

$$F = F_0 + \frac{\alpha}{2}P^2 + \frac{\beta}{4}P^4 + \frac{C}{2}S^4 - qP^2S - \frac{m}{2}P^2S^2 - PE \tag{2.3.1}$$

Here, F represents landau free-energy characterization of a ferroelectric, $F_0$ is independent of both polarization and strain, S represents strain. Using the relationship $\frac{\partial F}{\partial P} = 0$ and $T = \frac{\partial F}{\partial S}$, we can obtain the equations for Electric field(E) and Stress(T):

$$E = \frac{\partial F}{\partial P} = \alpha P + \beta P^3 - 2qPS - mPS^2 \tag{2.3.2}$$

$$T = \frac{\partial F}{\partial S} = cS - qP^2 - mP^2S \tag{2.3.3}$$

Applying the initial state of ferroelectric matrial (E=$E_{dc}$, T=0), and neglecting the nonlinear electrostriction controlled by m, we can obtain the relationship of $E_{dc}$ and $S_{dc}$with polarization:

$$E_{dc} = \alpha P_{dc} + \beta^* {P_{dc}}^3 \tag{2.3.4}$$

$$S_{dc} = q{P_{dc}}^2/c \tag{2.3.5}$$

where $\beta^* = \beta - 2q^2/c$.

Substituting dc component and ac component of the Electric field, Polarization, Strain and Stress into equation 2.3.2 and 2.3.3 and neglecting high-order ac terms, we can obtain the nonlinear constitute coupling equations of E, P, S, T:

$$E = \left(\alpha + 3\beta^* {P_{dc}}^2\right)P - 2qP_{dc}S \tag{2.3.6}$$

$$T = -2qP_{dc}P + (C - m{P_{dc}}^2)S \tag{2.3.7}$$

Substituting P in equation (2.3.6) and (2.3.7) using $P = D - \varepsilon^b E$ and writing the nonlinear constitutive equation in the form of linear constitutive equation, the nonlinear constitutive equation can be written as:

$$D = eS + \varepsilon^S E \tag{2.3.8}$$

$$T = c^E S - eE \tag{2.3.9}$$

where

$$\varepsilon^S = \varepsilon^b + \chi_f \tag{2.3.10}$$

$$\chi_f = \frac{1}{\alpha + 3\beta^* {P_{dc}}^2} \tag{2.3.11}$$

$$e = 2\chi_f q P_{dc} \tag{2.3.12}$$

$$c^E = c - (m + 4q^2\chi_f){P_{dc}}^2 \tag{2.3.13}$$

Appying the common parameters of Barium Strontium Titanite and tuning range of electric field to the above nonlinear constitutive equation, the stiffness ($c^E$) can be tuned by 4% with the electric field around $7*10^7 V/m$. The tuning range of stiffness of Barium Strontium Titanite

can also be observed and proved in the resonance frequency of tunable thin film Bulk Acoustic Wave Resonator based on Barium Strontium Titanite thin film. [11]

## 2.4 Structure Nonlinearity

Another way to generate nonlinearity stiffness is to create the structure nonlinearity on the substrate. In this work, we propose to dig holes on piezoelectric substrate to couple the parallel and perpendicular stiffness, therefore mechnical stiffess becomes a function of strain, and can be used to couple to electromagnetic energy to the propagating acoustic wave energy. The schematic figure is shown in Fig.2.4.1, and it represents the cross section of the substrate.

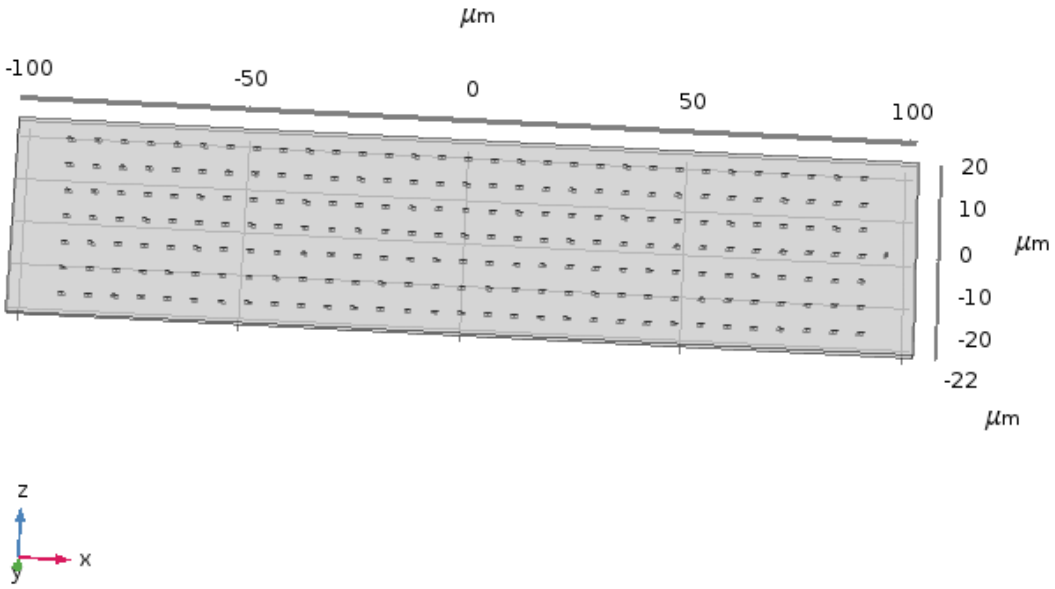


Figure 2.4.1 Schematic of nonlinear region created by structure

To derive the nonlinearity of this structure, we can use a simplified rod and spring model to represent this nonlinear structure as shown in Figure 2.4.2.

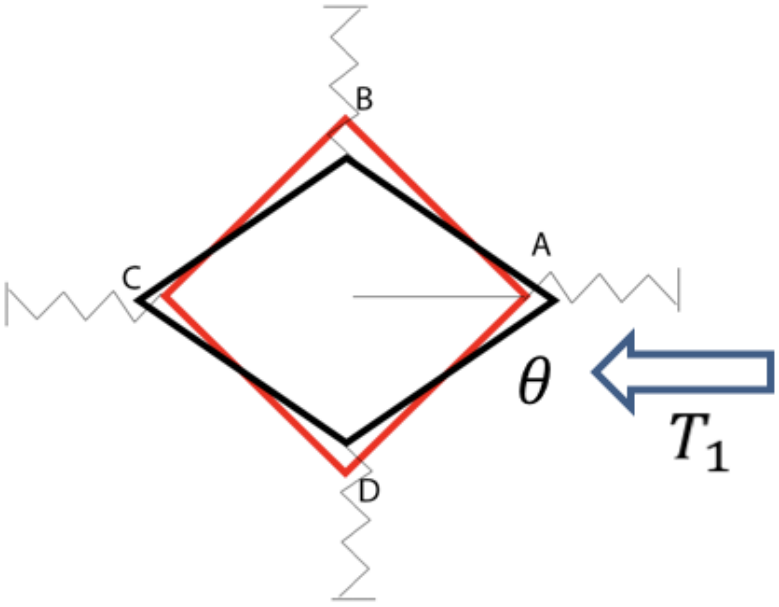


Figure 2.4.2 Simplified rods and spring model

Here, black lines represent the original state of hole, and the red lines represent the state after applying stress $T_1$. The springs in the figure represent the surronding material, and the rods represent the edges of the hole.

We can calculate the nonlinear mechanical stiffness by analyzing the force of A and B:

$$\begin{cases} T_1 - 2Tcos\theta = c_{11}S_1 \\ 2Tsin\theta = c_{22}S_2 \\ \Delta xcos\theta = S_1 l_1 cos\theta = S_2 l_2 sin\theta = \Delta ysin\theta \end{cases} \tag{2.4.1}$$

where T represents the stress on the rod between A and B, $\Delta x$ represents the displacement of point A, $\Delta y$ represents the displacement of point B, $l_1$ is the initial spring length of A, $l_2$ is the initial spring length of B, and $\theta$ represents the angle between rod and x direction as shown in the figure, l is the length of the edge between A and B.

From equation 2.4.1, we can write $T_1$ as a function of $S_1$, which is:

$$T_1 = (c_{11} + c_{22}\frac{l_1}{l_2}cot^2\theta)\, S_1 = c_{11}{}'S_1 \tag{2.4.2}$$

In order to find the relationship of $c_{11}{}'$ and $S_1$, we write $\theta$ as $\theta = \theta_0 + \Delta\theta$, and expand $c_{11}{}'$ near $\theta_0$. For simplicity, we neglect second and high order derivatives.

$$c_{11}{}' = \left(c_{11} + c_{22}\frac{l_1}{l_2}cot^2\theta_0\right) - \left(\frac{2c_{22}l_1cos\theta_0}{l_2sin^3\theta_0}\right)\Delta\theta \tag{2.4.3}$$

To find the relation between $\Delta\theta$ and $S_1$, following equations using geometrical relation can be obtained with the assumption that $\Delta\theta$ is very small:

$$\Delta\theta = \frac{\Delta x}{l}(sin\theta_0 + \frac{cos\theta_0}{\tan(\theta_0+\Delta\theta)} + cos\theta_0\Delta\theta) \tag{2.4.4}$$

After linearizing the equation,

$$\Delta\theta = \frac{\Delta x}{lsin\theta_0} = \frac{S_1 l_1}{lsin\theta_0}$$

Finally, we obtain the nonlinear relationship between Stress(T) and Strain(S):

$$T_1 = \left(c_{11} + c_{22}\frac{l_1}{l_2}cot^2\theta_0\right)S_1 - (\frac{2c_{22}{l_1}^2cos\theta_0}{ll_2sin^4\theta_0}){S_1}^2 \tag{2.4.5}$$

We can define $\xi$ as the modulation index to demonstrate the degree how the stiffness can be modulated.

$$\xi = (\frac{2c_{22}{l_1}^2cos\theta_0}{ll_2sin^4\theta_0})/\left(c_{11} + c_{22}\frac{l_1}{l_2}cot^2\theta_0\right) \tag{2.4.6}$$

The physical meaning of $l_1, l_2$ is shown in Fig. 2.4.3. $l_1$ is the distance between two nearby holes in the x direction, $l_2$ is the distance between two nearby holes in the z direction.

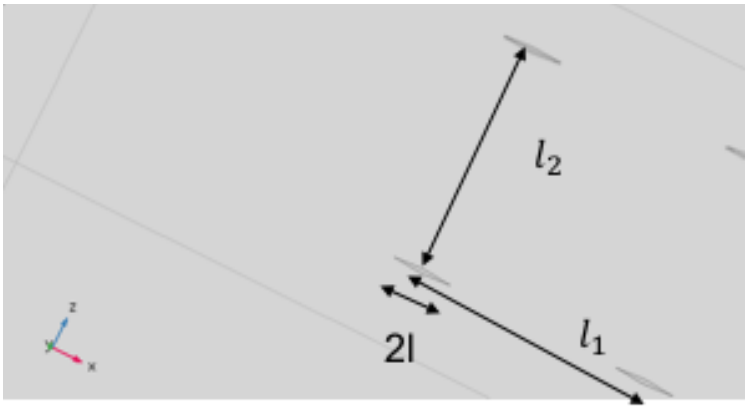


Figure 2.4.3 Hole size and hole gap

By substituting physical value of parameters in equation 2.4.5, the relationship between modulation index and strain with different hole geometry and hole gaps can be plotted as shown in Figure 2.4.4.

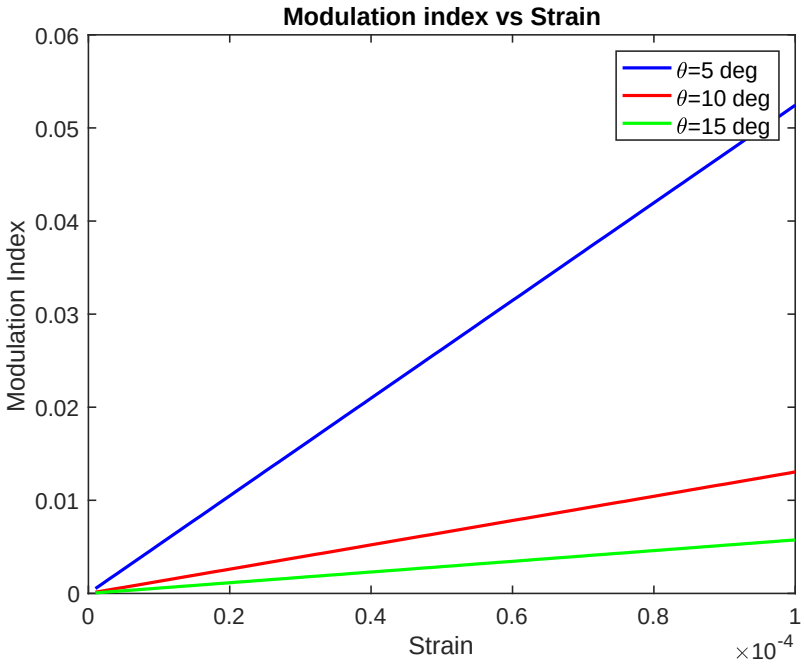


(a)

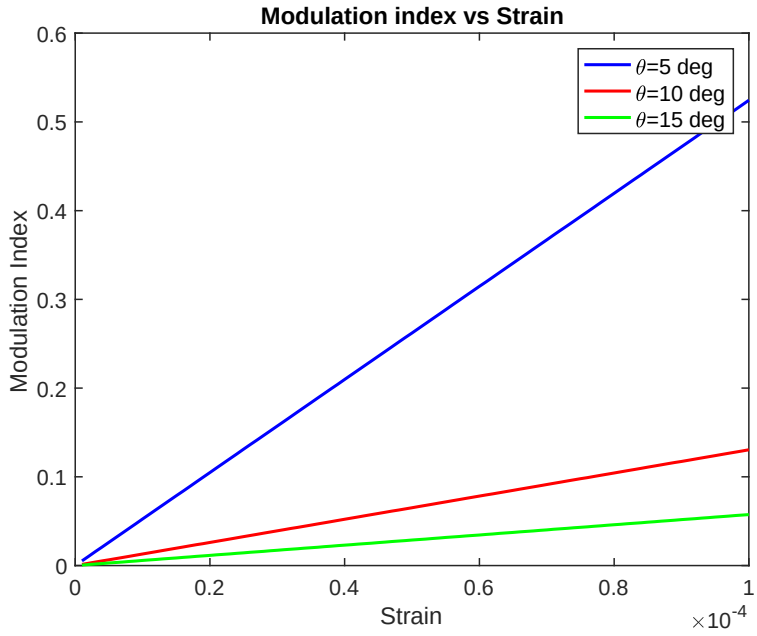


(b)

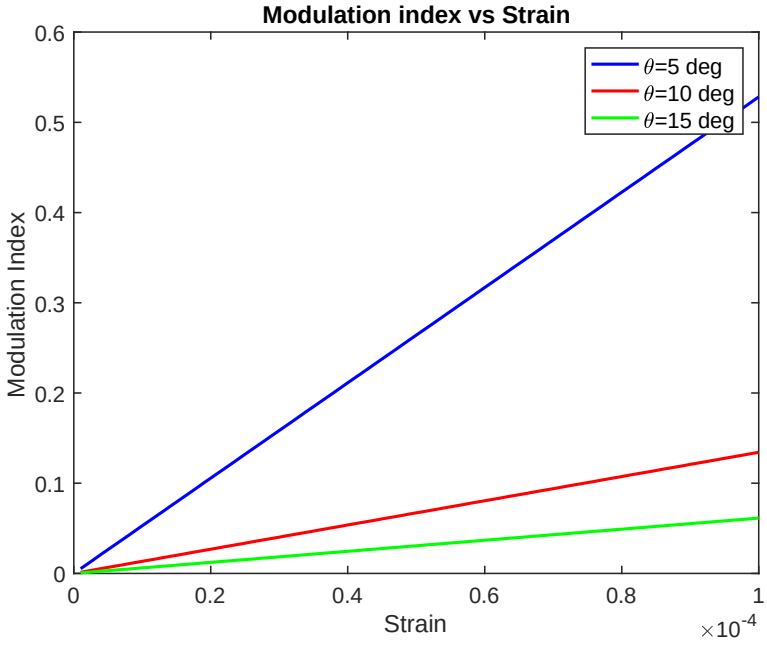


(c)

Figure 2.4.4 Relation between modulation index and strain with different angle and geometry of (a) $l_1 = 3um, l_2 = 3um, l = 1.5um$ (b) $l_1 = 3um, l_2 = 3um, l = 0.15um$ (c) $l_1 = 30um, l_2 = 3um, l = 1.5um$

From the plot, we can conclude that holes with shaper angle, smaller lengths and larger separation can provide larger modulation index for the parametric modulation. The criteria that limits the modulation index is the fabrication resolution, which prevents from obtaining large nonlinearity. Considerable nonlinearity, 10% or even higher, however, can be achieved from the geometry proposed in this work.

# CHAPTER 3

# Simulation of Surface Acoustic Wave Device

In this chapter, the simulation results about Surface Acoustic Wave using COMSOL Multiphysics are shown. The excitation of Surface Acoustic Wave is the first step for simulating Surface Acoustic Wave devices, which will be discussed in detail in the first part of this chapter. In order to overcome the losses for two ports Surface Acoustic Wave transducers in simulation, matching networking is developed and utilized. Based on the understanding of theory above, the simulation results of parametric amplification are demonstrated, which proves the parametric amplification concept in the surface acoustic wave platform using the nonlinear surface acoustic wave grating we proposed.

## 3.1 Excitation of Surface Acoustic Wave

The simulation tool for this work is COMSOL Multiphysics, which is a wide-used platform for electromagnetics, structural mechanics, acoustics, fluid flow, heat transfer, and chemical engineering behavior. The physics we are using in COMSOL is electrostatics and solid mechanics, and we can simulate the effects of external circuit on the Interdigital transducer (IDT), propagation of surface acoustic wave, and coupling between electrical energy and mechanical energy.

Surface acoustic wave can be excited by applying voltage on the Interdigital Transducer. The geometry of Interdigital Transducer is shown in the Fig. 3.1.1, the substrate material is YX-128° cut Lithium Niobate, the Interdigital Transducer material is Gold. The wave speed in YX-128° cut Lithium Niobate is 3895 m/s, the frequency for excited surface acoustic wave is 861MHz, the width and gap for each Interdigital Transducer is a quarter wavelength of the surface acoustic wave. The voltage excition is 1V which applied to the first, third, and fifth Interdigital Transducer from the left, and the ground is applied to the second, fourth, and sixth

Interdigital Transducer from the left. The electrostatics and solid mechanics physics are applied to all the regions in the geometry, the boundary condition for left, bottom, and right edge of the Lithium Niobate is low-reflection boundary.

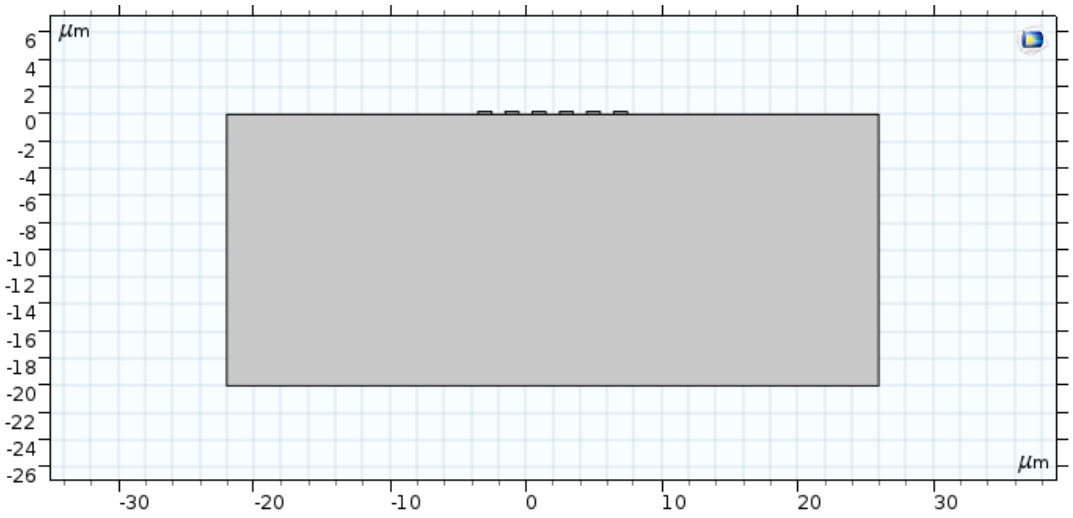


Figure 3.1.1 Geometry of Interdigital Transducer

We can run both time domain simulation and frequency domain simulation for exciting the surface acoustic wave, here we run time domain simulation to observe the propagation of surface acoustic wave. The displacement at three different time steps are shown in Figure 3.1.2, where we can observe the propagating pattern for surface acoustic wave.

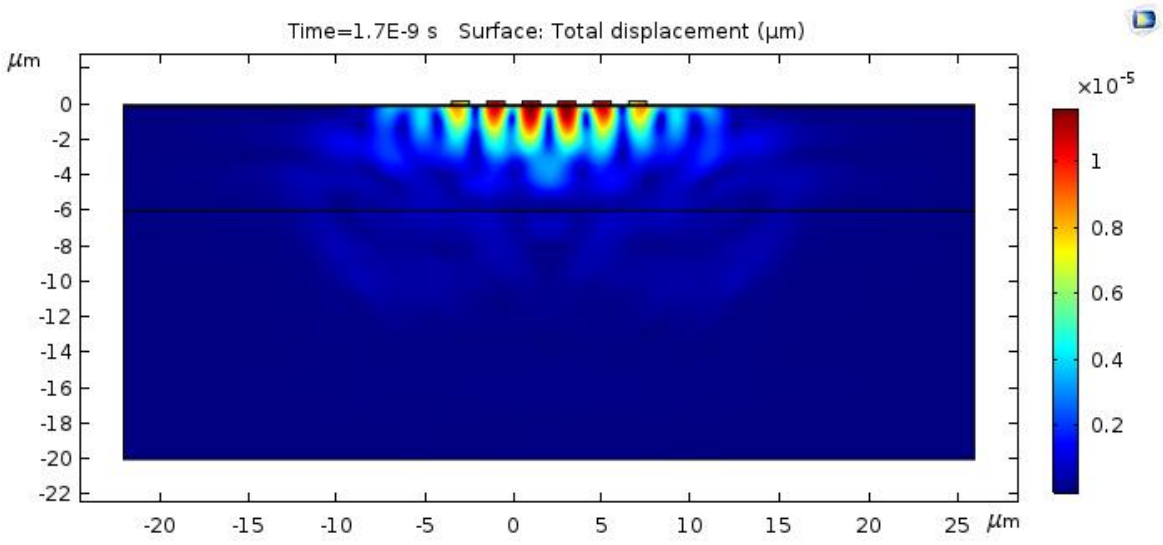

(a)

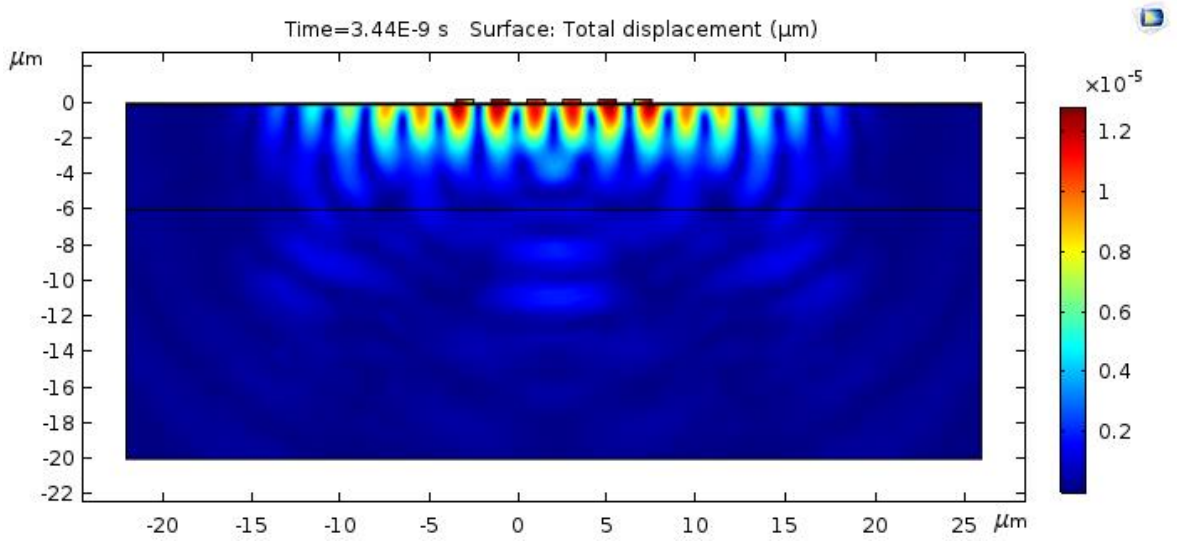


(b)

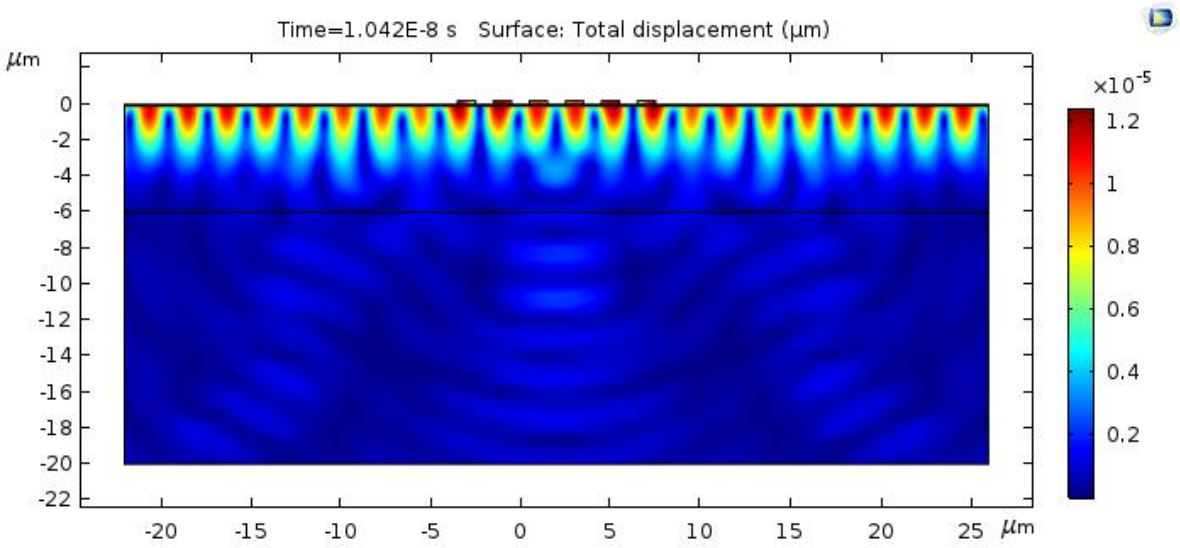


(c)

Figure 3.1.2 Displacement of surface acoustic wave at time step (a) $1.7 \times 10^{-9}$s (b) $3.44\times 10^{-9}$s (c) $1.042\times 10^{-8}$s

Besides displacement, we can also simulation strain, stress, and electric potential of surface acoustic wave. The strain(S11), stress(T11) and electric potential when surface acoustic wave reaches the boundary are shown in Figure 3.1.3. From the Figure 3.1.3(c), we observe that the

electric potential for surface acoustic wave is low, and it will cause large insertion loss for Surface Acoustic Wave delay line. Therefore, we will use the equivalent circuit of Interdigital Transducer for impedance matching in the following section.

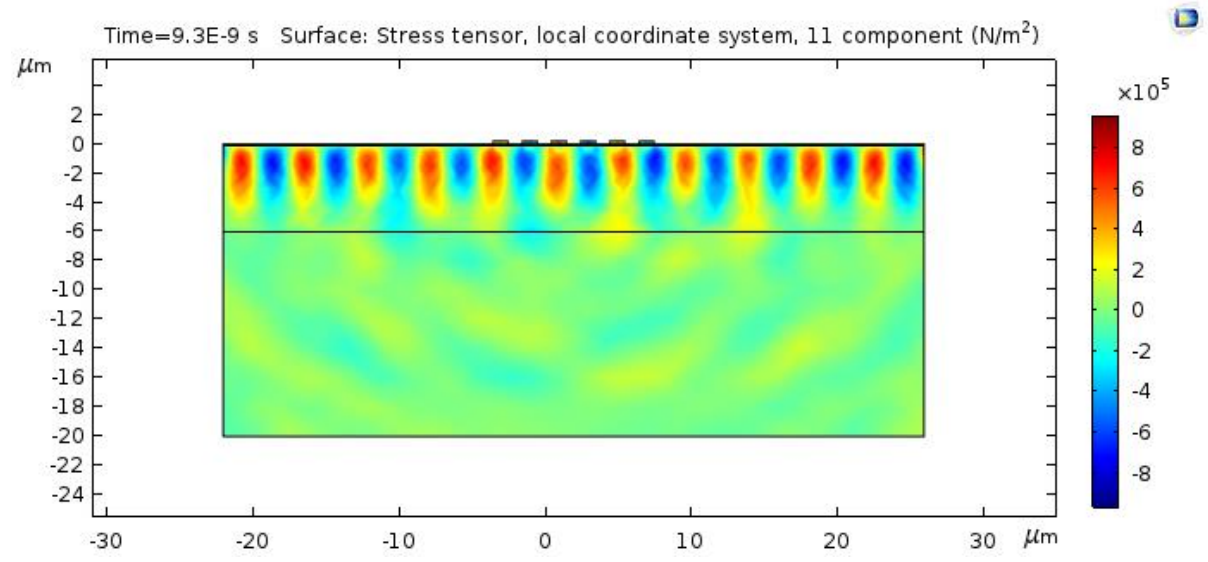


(a)

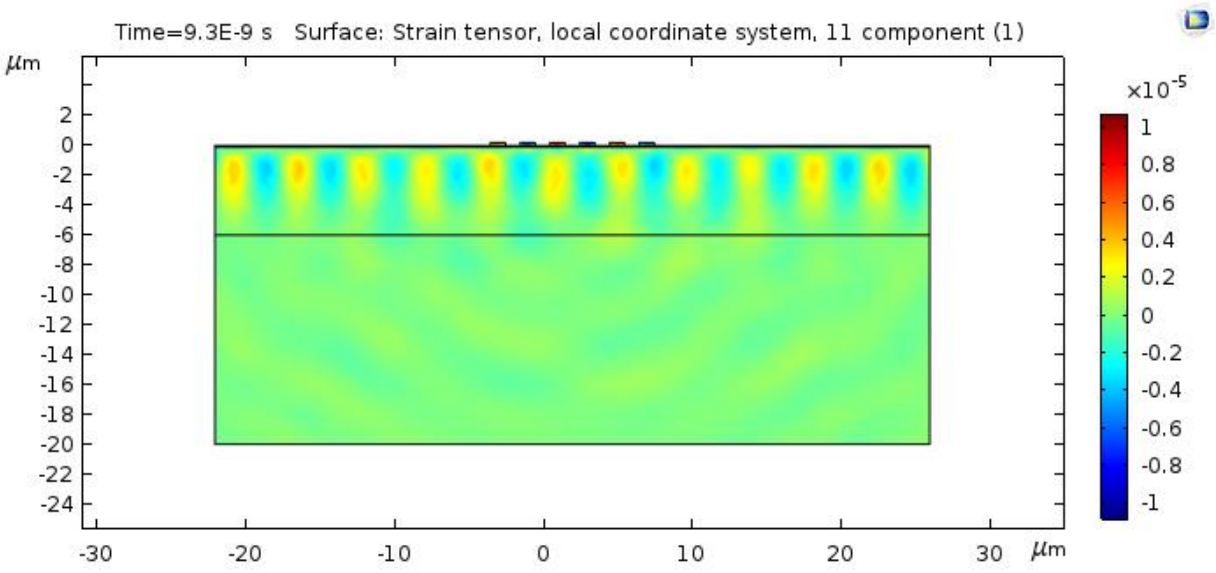


(b)

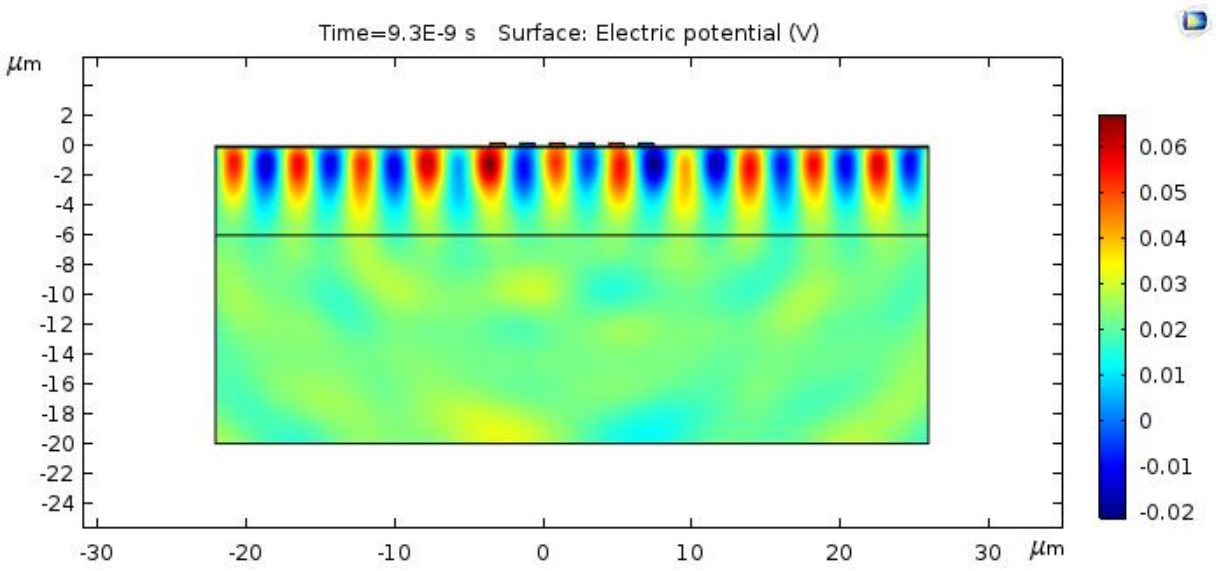


(c)

Figure 3.1.3 (a) Strain (S11) (b) Stress (T11) (c) Electric potential at time step $9.3 \times 10^{-9}$s

## 3.2 Impedance Matching for Interdigital Transducer

Mason circuit has been widely used for modeling Surface Acoustic Wave Interdigital Transducer [13]. The mason model equivalent circuit for one periodic section of Interdigital Transducer is shown in Figure 3.2.1. Here, port 3 represents the electrical input, $c_s$ is the electrode capacitance per section, transformer represents the electromechanical coupling between electromagnetic wave and acoustic wave. Piezoelectric substrate for the propagation of Surface Acoustic Wave can be modelled by transmission line, which is inductor and capacitor in the Figure 3.2.1. Because Surface Acoustic Wave can travel in both directions in the substrate, so the network is actually three ports with two acoustic ports.

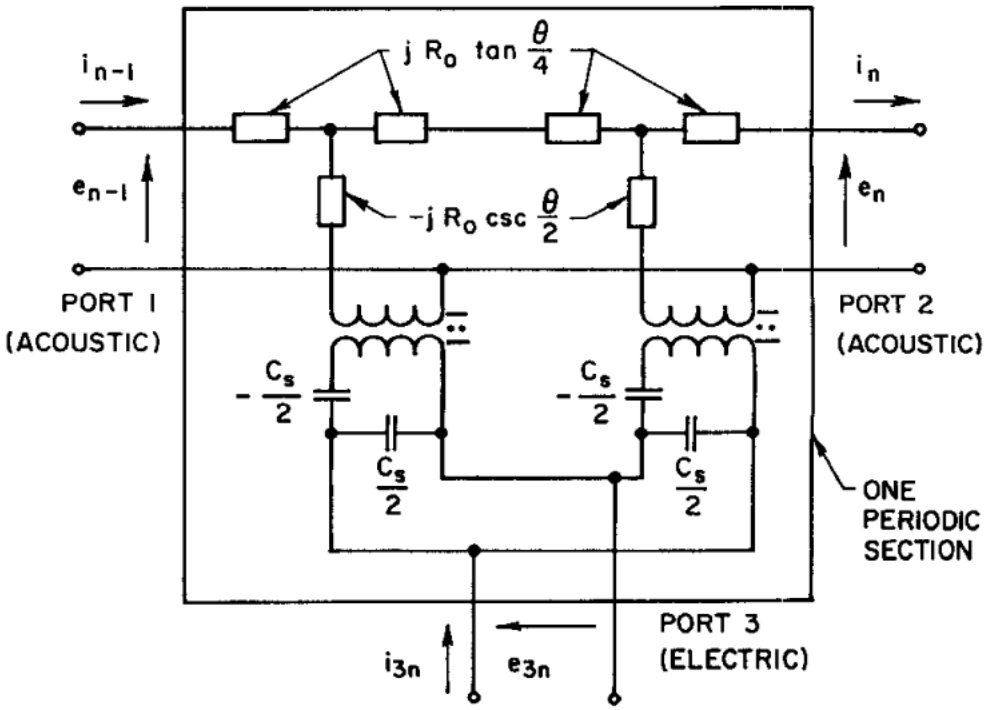


Figure 3.2.1 Mason equivalent circuit for one period section

Mason equivalent circuit helps much on understanding the physics. Based on this, we develop a straightforward equivalent circuit for impedance matching two ports Surface Acoustic Wave Interdigital Transducers as shown in Figure 3.2.2. Here, one set of Interdigital Transducer is for exciting the Surface Acoustic Wave (input), one set of Interdigital Transducer is for transforming the mechanical wave into electromagnetic wave(output). We can put the two ports Surface Acoustic Wave Interdigital Transducers into a black box, and use Z matrix to represent its characteristic. This method can be applied in designing the matching LC circuit. Because the two ports Surface Acoustic Wave Interdigital Transducers are identical, we can use same matching circuit in the source and load. $R_s$ and $R_L$ are the source resistor and load resistor (usually 50 Ohm), respectively.

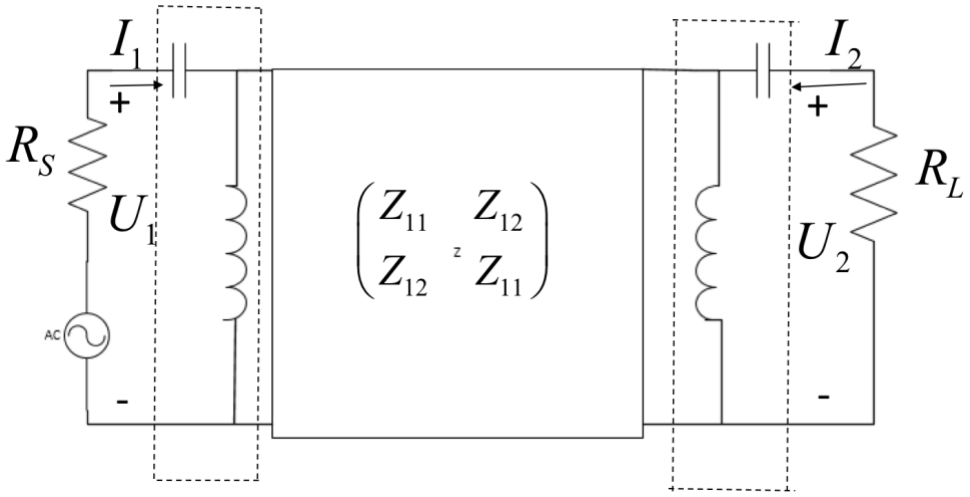


Figure 3.2.2 Impedance matching network for two ports Surface Acoustic Wave Interdigital Transducer

In order to design the matching circuit, we build two ports Surface Acoustic Wave Interdigital Transducers in COMSOL Multiphysics with one set of input Interdigital Transducer and one set of output Interdigital Transducer, as shown in Figure 3.2.3.

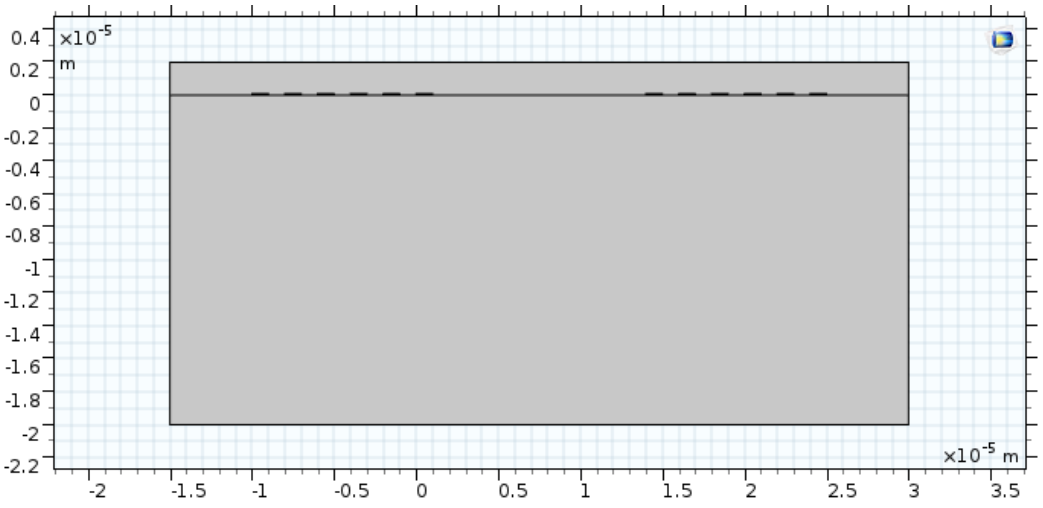


Figure 3.2.3 Geometry of two ports Interdigital Transducer

We can add external circuit to the Interdigital Transducers by Electrical Circuit Module in COMSOL. For determining the value of inductor and capacitor in the matching circuit, we first measure the voltage $U_1$ on the input Interdigital Transducer, and the current $I_1$ flowing into the network, when the output Interdigital Transducer is open-circuited. The real part and

imaginary part of the input impedance of Interdigital Transducer is shown in Figure 3.2.3. The real part is 14Ohm at 973.75MHz, with imaginary part -27Ohm. The real part at the resonance frequency is caused by the energy coupling, the imaginary part is due to static capacitance of the electrodes.

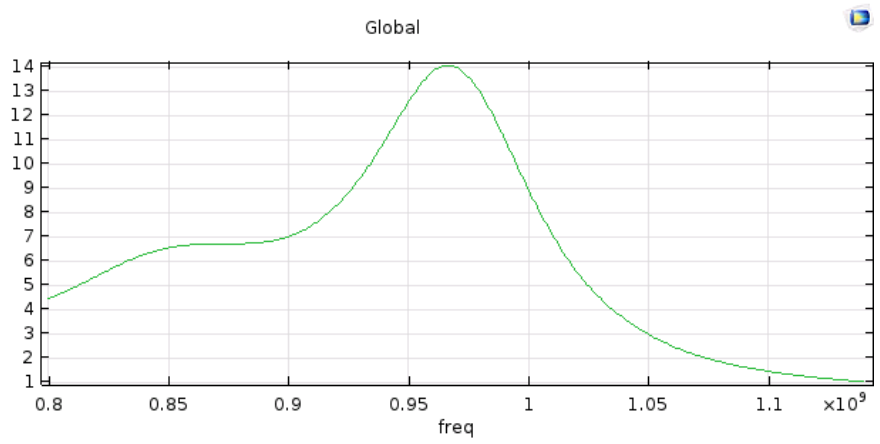


(a)

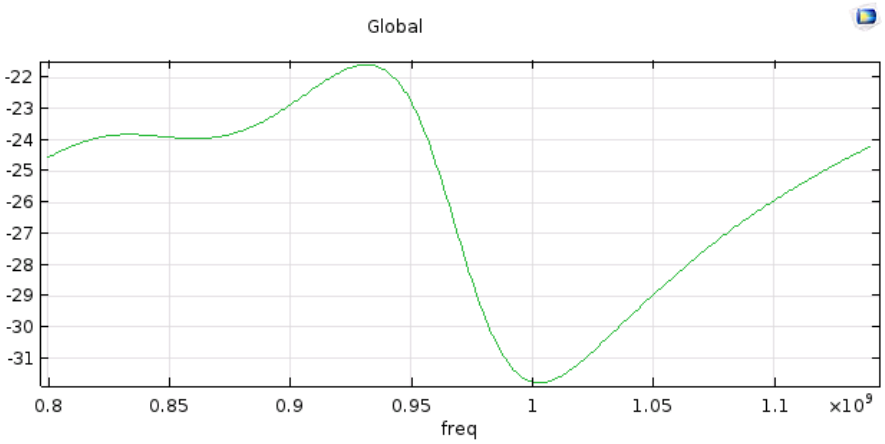


(b)

Figure 3.2.4 (a) Real part and (b) Imaginary part of input impedance of Interdigital Transducer

With these values, we can design the matching circuit using smith chart [14]. The series capacitor is 6.5378pF, the parallel inductor is 4190.9pH. By adding the matching LC circuit on both ports, larger output electrical power can be obtained at output Interdigital Transducer. Figure 3.2.5(a) shows the voltage excitation on the input Interdigital Transducer and induced

voltage on the output Interdigital Transducer, and Figure 3.2.5(b) shows the current flowing into the input Interdigital Transducer and current flowing out from the output Interdigital Transducer. Almost 6~8 dB insertion loss can be observed in the two ports Interdigital Transducers configuration, which is the theoretical limit of this simple Surface Acoustic Wave Delay line configuration. 3dB insertion loss happens at both input and output transducer because the acoustic wave can travel in two directions. This impedance matching technique is very helpful in developing the matching circuit for Surface Acoustic Wave devices in simulation, with guidance on the fabrication of Surface Acoustic Wave devices.

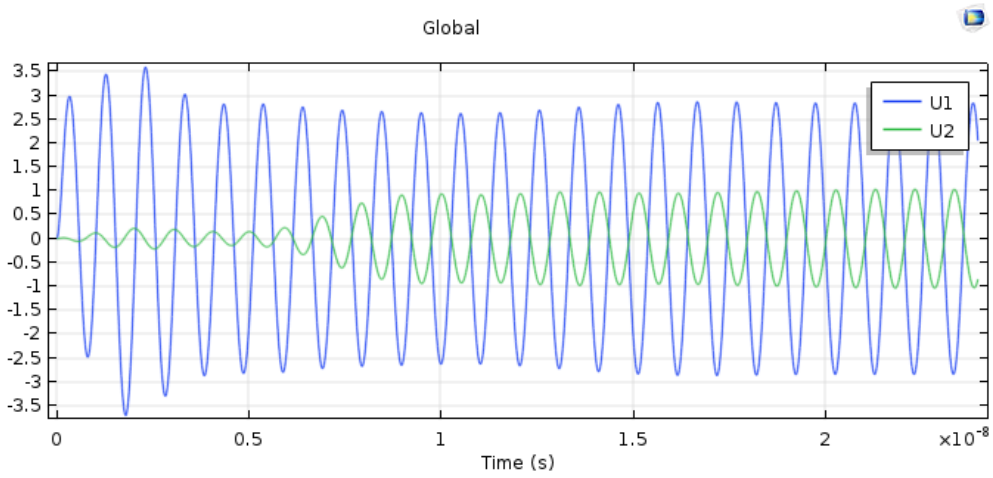


(a)

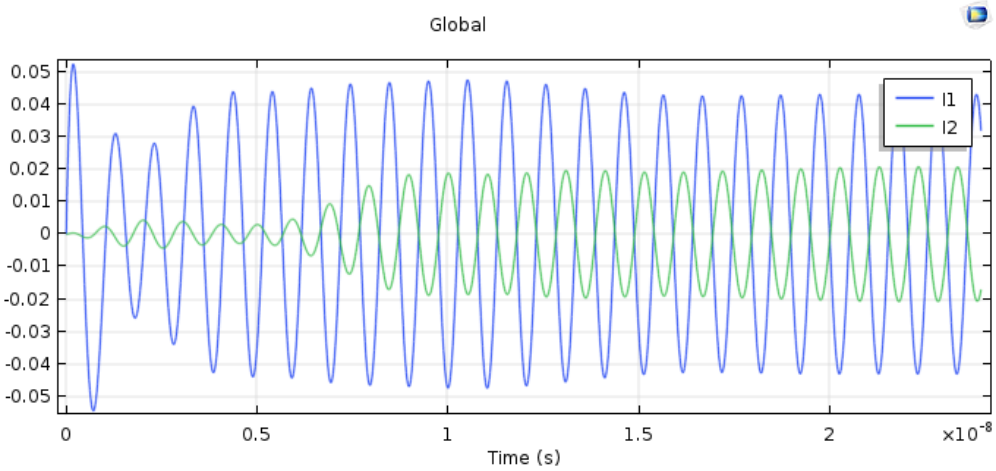


(b)

Figure 3.2.5 Comparison of (a) Voltage Excitation and Output Voltage (b) Input Current and Output Current

## 3.3 Parametric Modulation in Surface Acoustic Wave Simulation

The proof of parametric modulation concept will be demonstrated in the COMSOL simulation in this section, with the help of Time Varying Transmission Line theory and equivalent circuit for Surface Acoustic Wave Interdigital Transducer mentioned in the above sections. The geometry and setup of parametric modulation is shown in Figure 3.3.1.

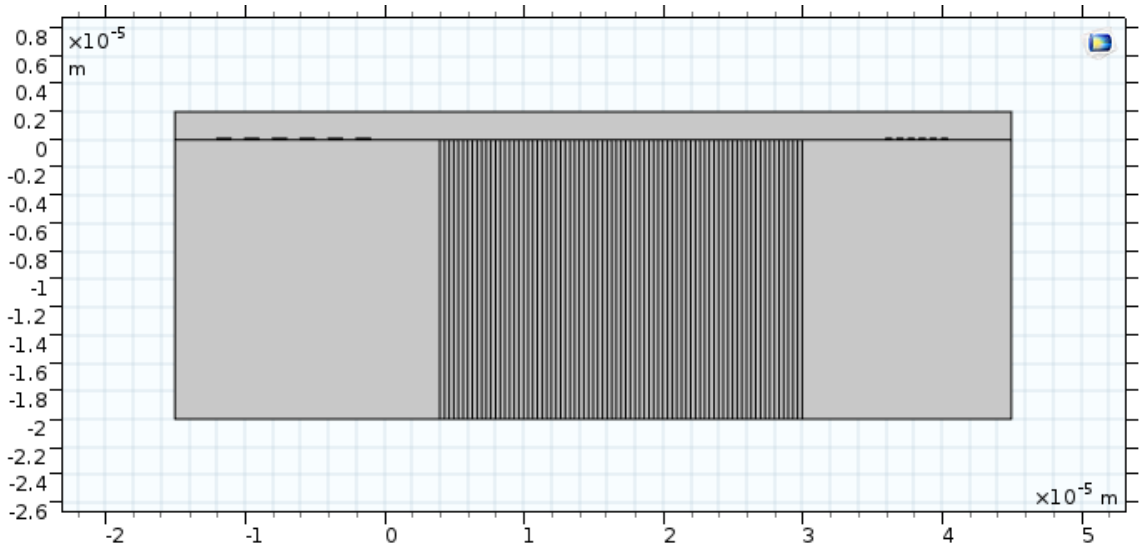


Figure 3.3.1 Geometry of Parametric modulation in Surface Acoustic Wave Simulation

The Input Interdigital Transducer is designed at $f_s = 974MHz$, with the excitation of surface acoustic wave as signal wave. The output Interdigital Transducer is designed at $f_{p+s} = 2434MHz$, which is used for detecting up-converted surface acoustic wave at this frequency. Modulation region is in the middle of the substrate, the total length of modulation region is $7\lambda_p$. Analogous to Time Varying Transmission Line, the mechanical stiffness of this modulation region can be varied by carrier electromagnetic wave which is $f_p = 1460MHz$ in this simulation. The modulation index is 0.1, implying the change of mechanical stiffness in

this modulation region is 0.1. The layers in the modulation region introduce phase delay to the electromagnetic wave, which contribute to the phase matching condition for parametric modulation between electromagnetic wave and surface acoustic wave. The displacement of Surface Acoustic wave in this simulation at time step $5 \times 10^{-8} s$ is shown in Figure 3.3.2, with the mixing phenomenon happening in the middle modulation region. We can observe Surface Acoustic Waves of different wavelength in and after the modulation region, which demonstrate the parametric effects.

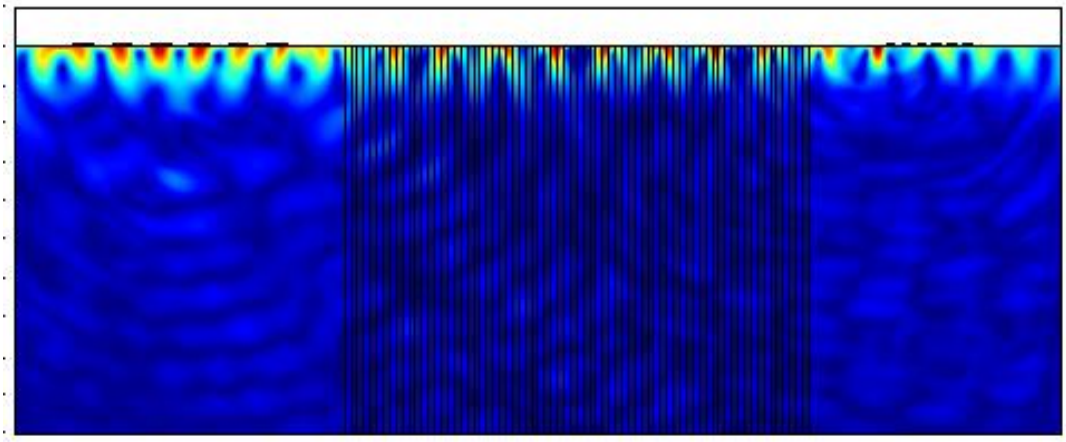

Figure 3.3.2 Displacement of the Surface Acoustic Wave in the simulation

To quantize the parametric modulation effects, the induced voltage on the Interdigital Transducer is plotted in time domain and analyzed in the frequency domain using Fast Fourier Transform as shown in Figure 3.3.3. Mixing effects can be clearly observed in the Figure 3.3.3(a). Frequency domain analysis shows the signal surface acoustic wave ($f_s = 974MHz$) and the up-converted surface acoustic wave $f_{p+s} = 2434MHz$, which further proves the parametric concepts using nonlinear surface acoustic wave grating.

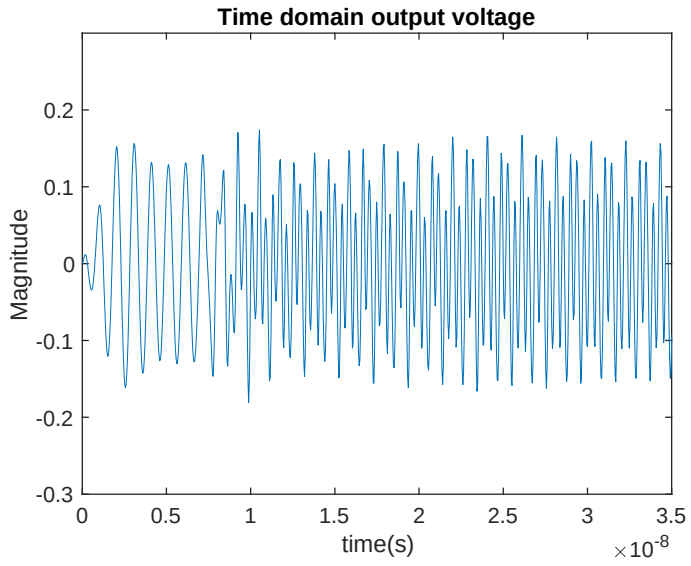


(a)

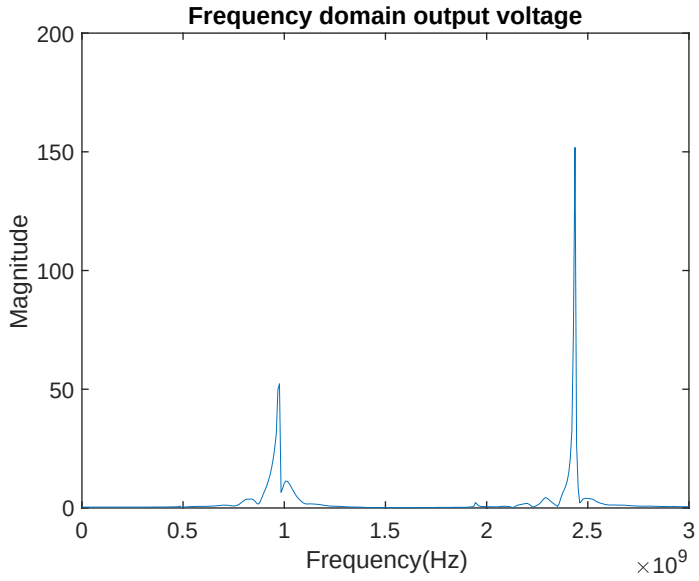


(b)

Figure 3.3.3 Output Voltage in (a)Time domain and (b) Frequency domain

If we vary the total length of modulation region, we can observe the change of magnitude of up-converted surface acoustic wave, which corresponds to the solution of Time Varying Transmission Line derived in the equation (2.1.4.3). The output voltages of Interdigital

Transducer in frequency domain when total length of modulation region is $9\lambda_p$ and $11\lambda_p$ are shown in Figure 3.3.4.

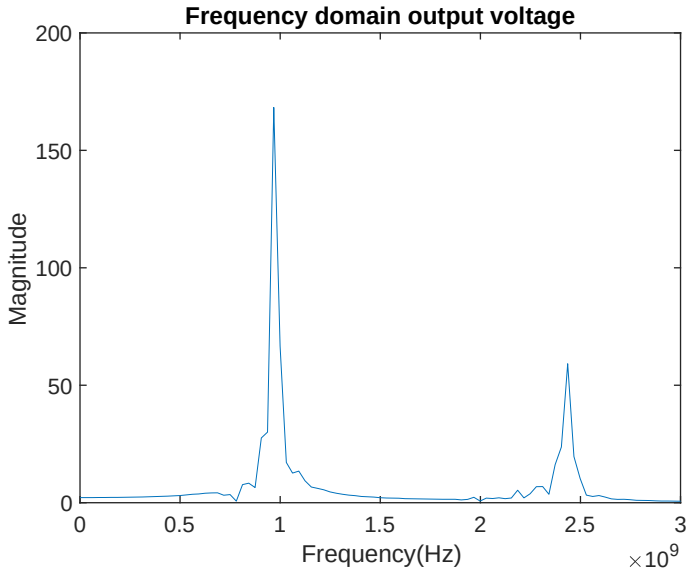


(a)

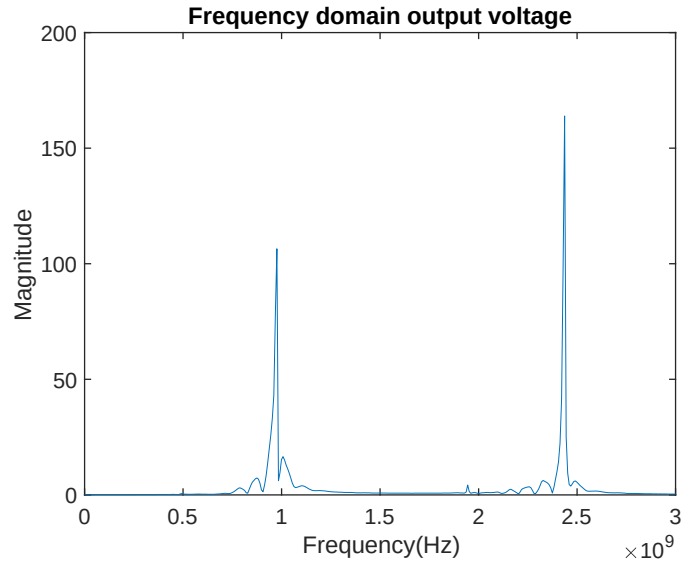


(b)

Figure 3.3.4 Output voltage in Frequency Domain with length of modulation region (a) $9\lambda_p$ (b) $11\lambda_p$

Magnitude of up-converted surface acoustic wave in theory and in simulation is compared and plotted in Figure 3.3.5. The simulation results fit the theory very well. The highest conversion gain is achieved when length of the modulation region is $10\lambda_p$, and the trend will repeat itself, because the solution for time varying transmission line is a sine function.

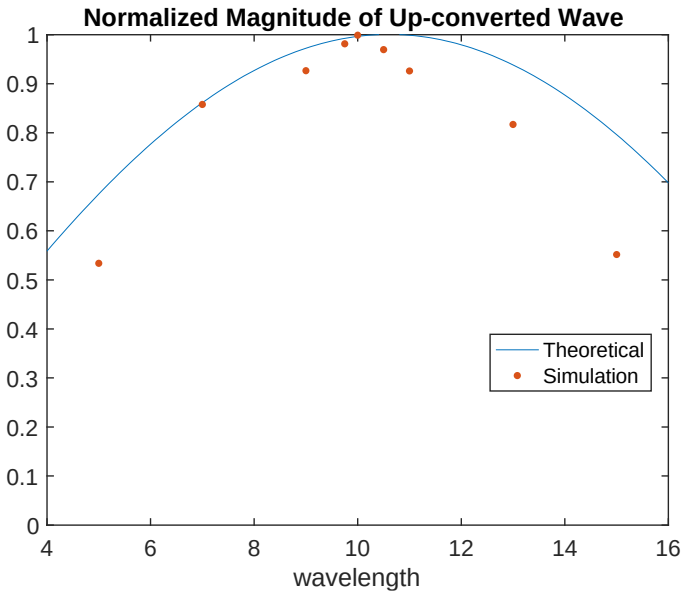


Figure 3.3.5 Normalized magnitude of up-converted surface acoustic wave in theory and simulation

# CHAPTER 4

# Fabrication and Characterization of Surface Acoustic Wave Device

In this chapter, the fabrication process for surface acoustic wave delay line and characterization of the fabricated devices performance will be demonstrated. The measurement results prove good performance of our device if with impedance matching, which serve as solid foundation for future works.

## 4.1 Fabrication of Surface Acoustic Wave Device

The fabrication process of surface acoustic wave delay lines is developed in the Integrated Systems Nanofabrication Cleanroom and Nanolab of University of California, Los Angeles. The process includes photolithography, metal deposition and lift off, which will be discussed in the following paragraphs.

The piezoelectric substrate we use for exciting surface acoustic wave is YX-128° Lithium Niobate thin film, which is cleaned using Matrix 105 – Downstream Ashier in Figure 4.1.1 and dehydrated using hot plate at 100 ℃ for 10 minutes in the Integrated Systems Nanofabrication Cleanroom. After that, the substrate is cooled down for 5 minutes before spinning the photoresists.


Figure 4.1.1 Matrix 105 – Downstream Ashier

HDMS and AZ nLOF 2020 are the chosen photoresists, which are deposited on the Lithium Niobate subctrate using Headway PWM32 – Spin Coater shown in Figure 4.1.2. First the HDMS is put on the top of substrate with a pipe, spinning at 500 rpm spin speed with 500 rpm/s spin ramp for 5 seconds, followed by 3000 rpm spin speed with 500 rpm/s spin ramp for 60 seconds. Secondly the AZ nLOF 2020 is spinning at 500 rpm spin speed with 500 rpm/s spin ramp for 5 seconds, followed by 3000 rpm spin speed with 500 rpm/s spin ramp for 60 seconds.


Figure 4.1.2 Headway PWM32 – Spin Coater

After covering the sample with photoresists, the sample is placed at the hot plate for 1 minute's soft bake before cooling down. The sample and the mask are then placed on Karl Suss MA6 Contact

Aligner in the Integrated Systems Nanofabrication Cleanroom shown in Figure 4.1.3 for exposure. The photomask is drawn using L-edit and made by Heidelberg DW66 Laser writer in the Nanolab. The exposure time is 7.7 second with 8.5 mW power, which should be adjusted by the exact power shown on the machine. After exposure, the sample is placed on the hot plate at 110℃ for 1 minute's post exposure bake.

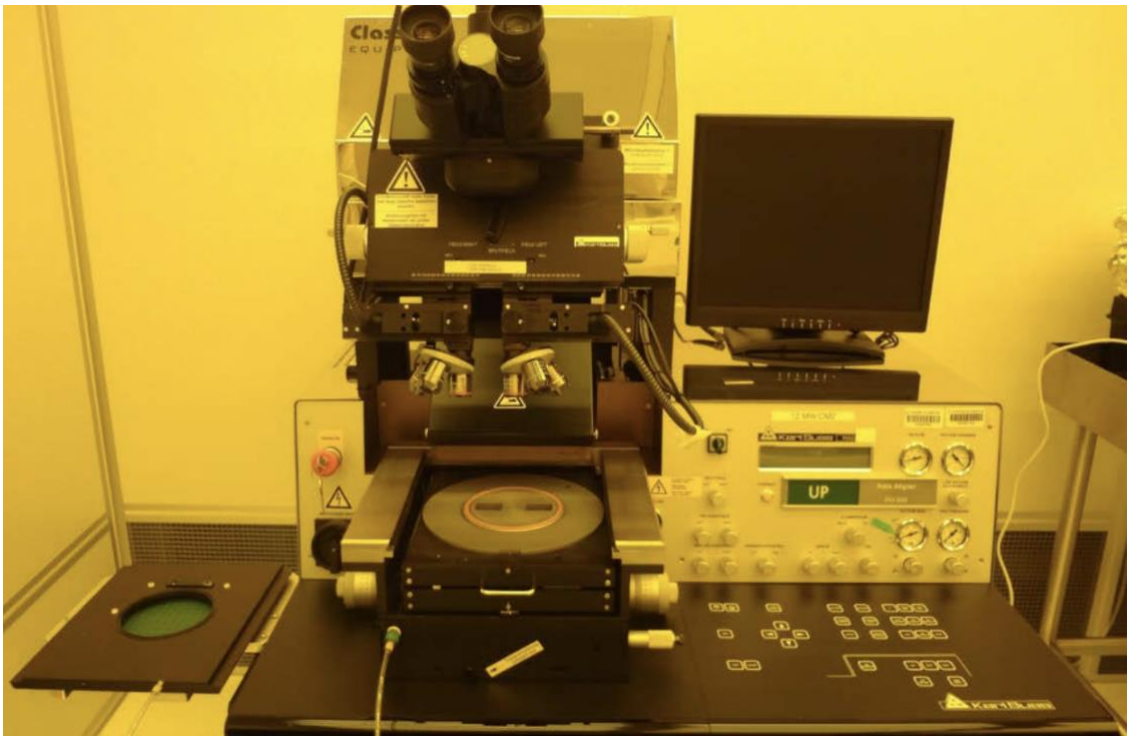


Figure 4.1.3 Karl Suss MA6 Contact Aligner

Before depositing the metal on the sample, the photoresist should be developed to obtain the pattern we want. In the develop process, the sample is immersed in a beaker with half MIF 300 for 50 seconds. Photoresists that are exposed by the UV Light become soluble in the solvent. After developing, the wafer is cleaned again before metal deposition.

The material for interdigital transducers and gratings of the Surface Acoustic Wave Delay Line is Aluminum deposited by CHA Mark 40 Electron Beam Evaporator in the Nanolab as shown in Figure 4.1.3. The thickness of the Aluminum deposited is 70nm, which is precisely controlled by the crystal in the Electron Beam Evaporator equipment.

Figure 4.1.4 CHA Mark 40 Electron Beam Evaporator

For the lift off process, the sample is immersed in a beaker of half NMP with Al Foil covering on the low speed Orbit-shaker for one night. During the liftoff process, photoresist will become soluble in the solvent, and metal on the photoresist will be moved by the photoresist. In this way, the pattern is transferred from photoresist to metal.

The final chip after the whole fabrication process is shown in Figure 4.1.5, with each pattern on the chip representing one surface acoustic wave delay line. Comparison of the size between chip and coin is shown, proving that the surface acoustic wave devices have much smaller device size than electromagnetic wave devices.

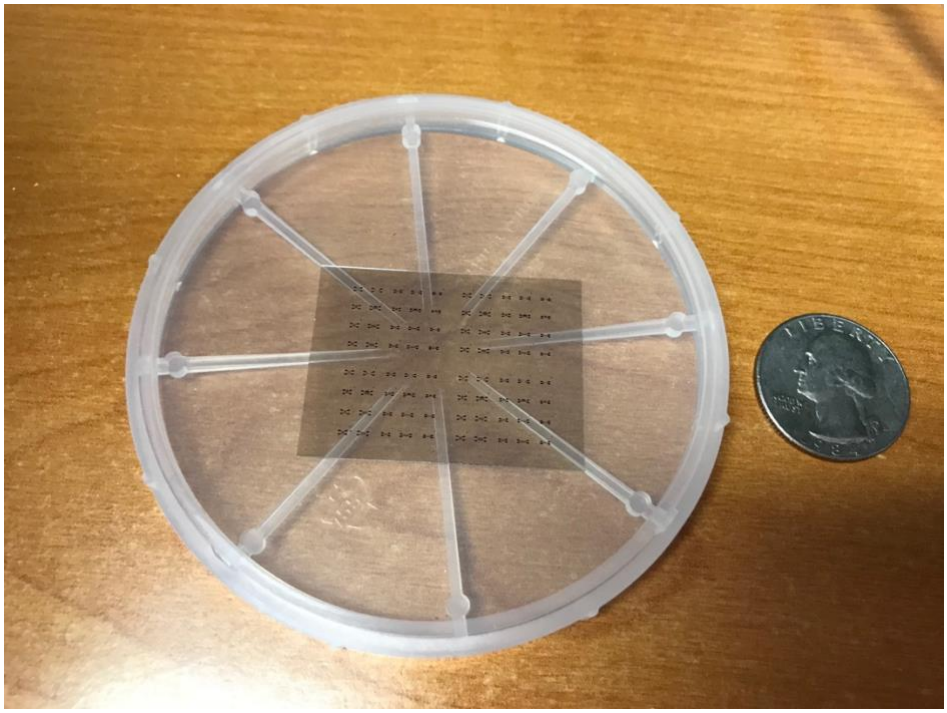

Figure 4.1.5 Final chip after whole fabrication process

Images of surface acoustic wave delay lines under optical microscope with different lenses are shown in Figure 4.1.6. There will be defects in one or two surface acoustic wave devices for every chip, but overall the devices are fabricated as expected, with fine and clean patterns of electrodes. The measurement results of these surface acoustic wave devices are shown in the following section.

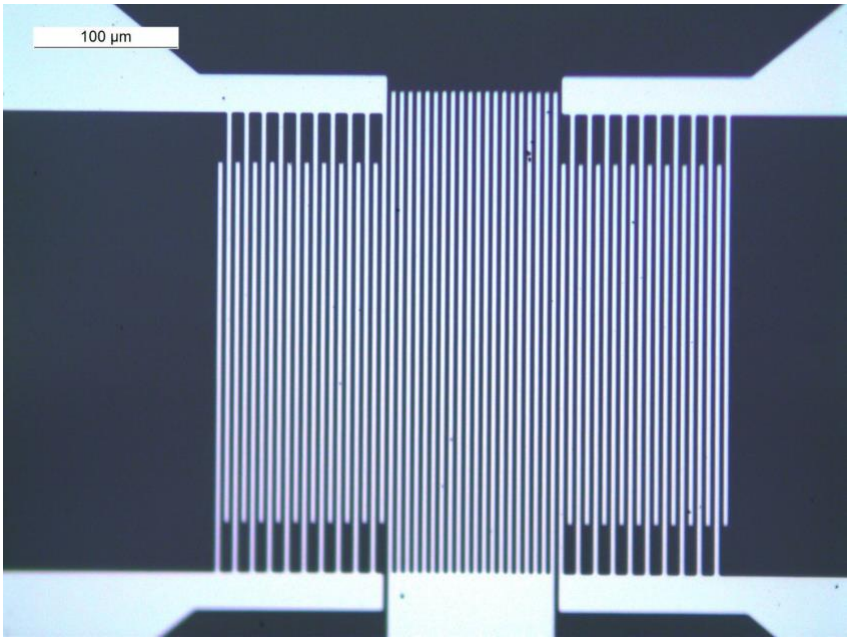

(a)

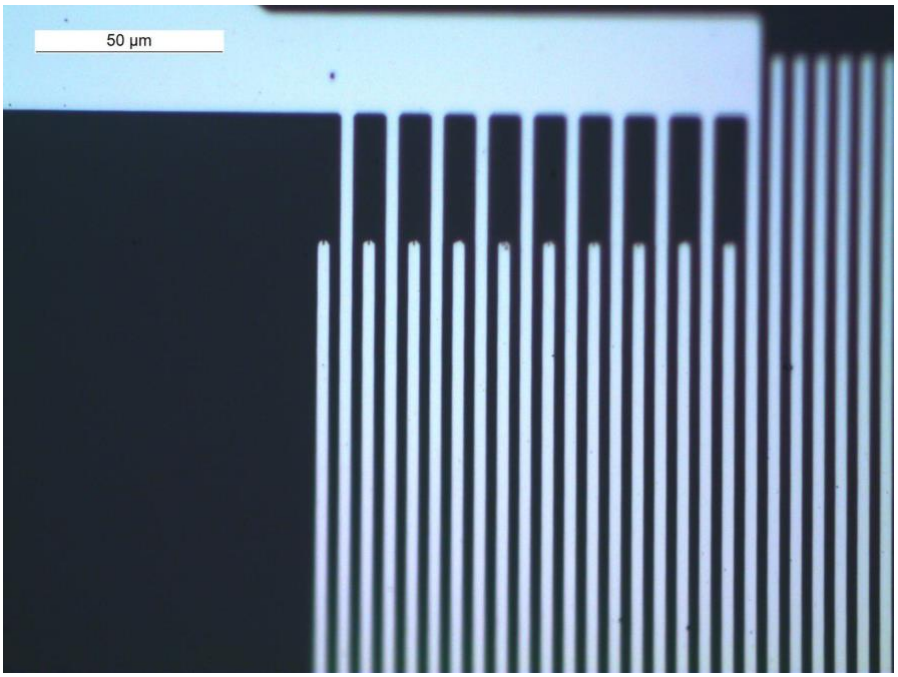


(b)

Figure 4.1.6 Images of surface acoustic wave delay lines

## 4.2 Characterization of Surface Acoustic Wave Device

The PCB for testing the surface acoustic wave devices is shown in Figure 4.2.1, which is drawn and simulated in Advanced Design System (ADS) before being cut by the LPKF ProtoLaser machine in the center for High Frequency Electronics in UCLA. Because the size of each surface acoustic wave device is very small, we put four surface acoustic wave devices on the same PCB and test them.

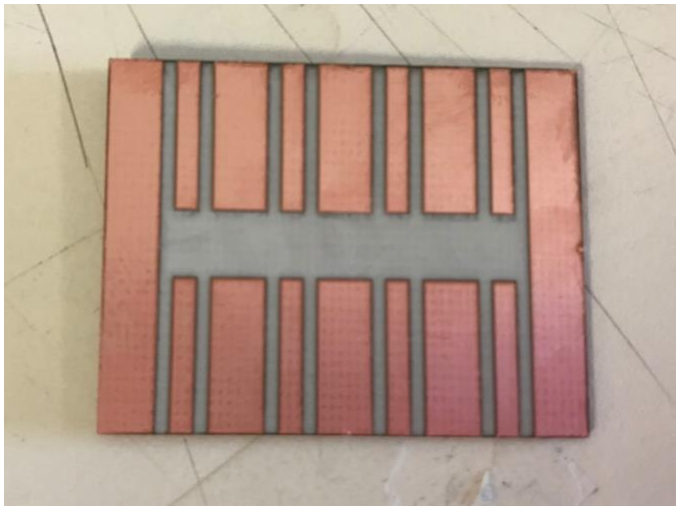

Figure 4.2.1 PCB cut by Laser Machine

The SMA connectors are wire bonding to the PCB before pasting the chip on the PCB using tape. The chip fabricated in the clean room is diced and wire bonding to the PCB by the center for High Frequency Electronics in UCLA. The final design for measurement is shown in Figure 4.2.2, with each set of SMA connected to the two feeding pads of the surface acoustic wave delay lines.

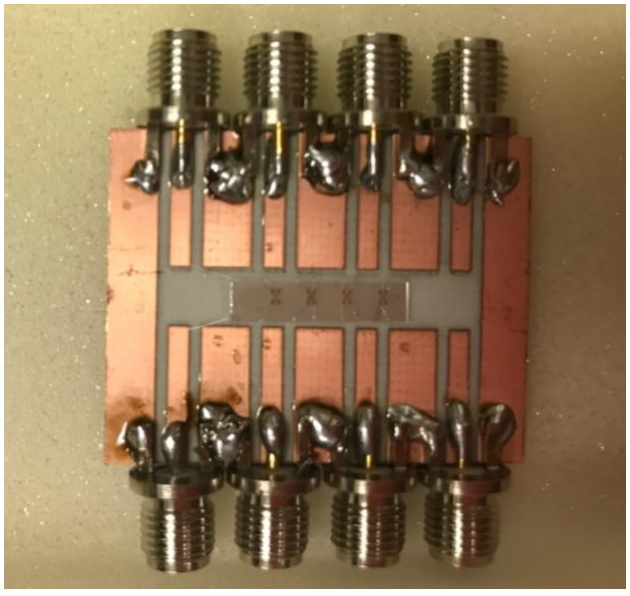

Figure 4.2.2 Device for testing

The characterization of the surface acoustic wave delay lines is performed on the Performance Network Analyzer–X in the Active Materials Laboratory. Calibration is performed before measuring the devices. We have measured nearly eight different surface acoustic wave devices of

our design. They vary in the length of electrode and total distance of grating, which will affect their measurement performance. The Return Loss (S11) and Insertion loss (S21) of one surface acoustic wave device is shown in Figure 4.2.3. As illustrated in the figure, the insertion loss is larger than the simulation, the reason of which is the impedance difference between simulation and measurement. Most of the power is reflected at the input interdigital transducer and not transmitted into the network.

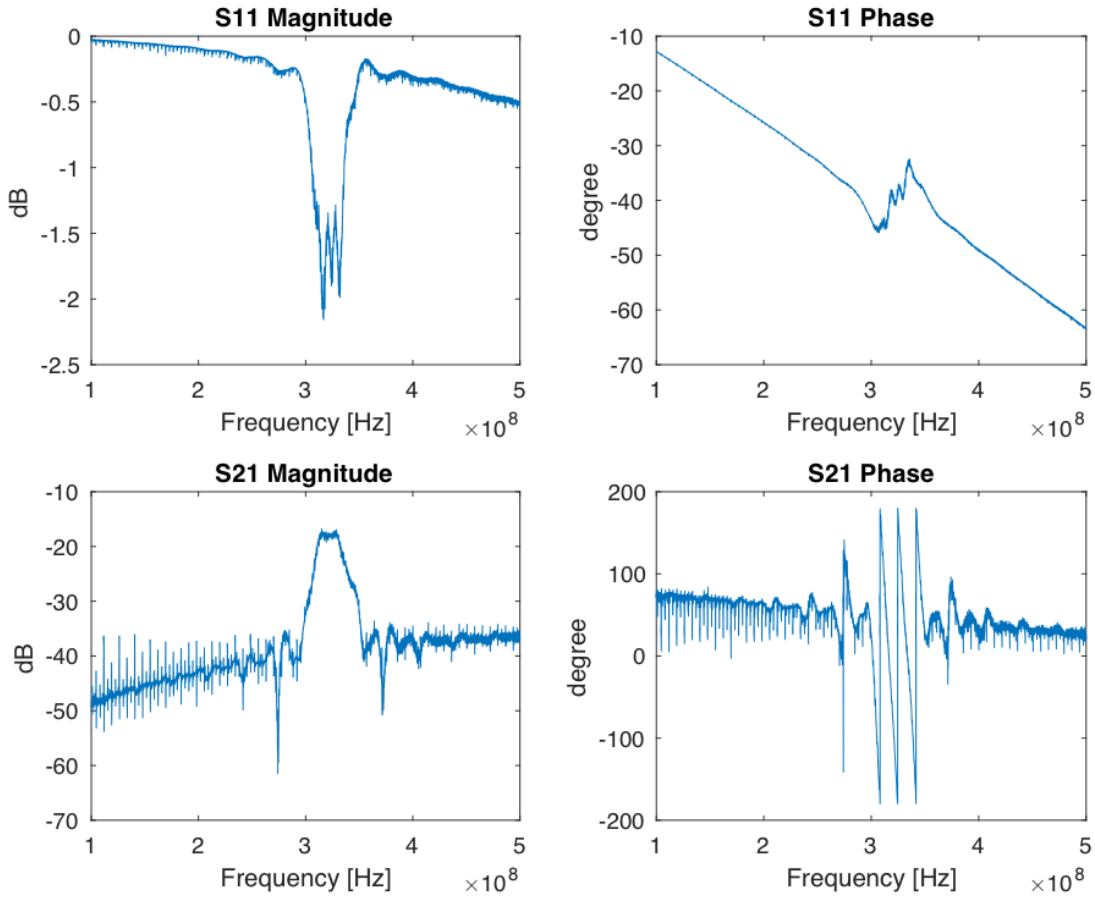


Figure 4.2.3 Measurement results

To solve this issue and reduce the insertion loss, impedance matching is used to eliminate the reflected power at the input and output. Advanced Design System (ADS) is used to design the matching circuit for the measured data. The return loss and insertion loss after applying the matching circuit is shown in Figure 4.2.4. The insertion loss is -6dB at desired frequency, which is

almost the limit of the theoretical insertion loss, demonstrating the low propagation loss of surface acoustic wave device we make. The fabrication and characterization technique will be used later for surface acoustic wave devices with parametric amplification.

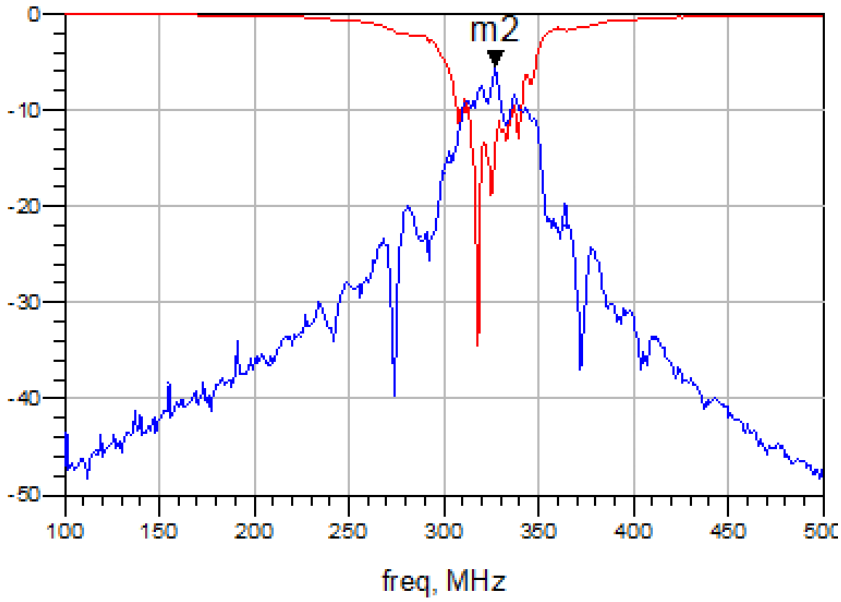


Figure 4.2.4 Return Loss and Insertion Loss after Impedance Matching

# CHAPTER 5

# Conclusion

## 5.1 Summary

The concept of parametric amplification on the surface acoustic wave platform using nonlinear surface acoustic wave grating has been proposed and proved in simulation. The methods to realize nonlinear mechanical stiffness modulation has been well illustrated. The fabrication and characterization of surface acoustic wave devices provide solid foundation for the following experiments with parametric modulation.

## 5.2 Future Work

Although the concept of parametric amplification on the surface acoustic wave platform using nonlinear surface acoustic wave grating has been proved in simulation, more work should be done to test the surface acoustic wave device with parametric amplification. Also, alternative methods to create nonlinearity in mechanical stiffness modulation are preferred for obtaining better parametric performances.

# REFERENCES


[1] Qin, Shihan, Qiang Xu, and Yuanxun Ethan Wang. "Nonreciprocal components with distributedly modulated capacitors." *IEEE Transactions on Microwave Theory and Techniques* 62.10 (2014): 2260-2272

[2] Qin, Shihan, and Yuanxun Ethan Wang. "Broadband parametric circulator with balanced monolithic integrated distributedly modulated capacitors (DMC)." *Microwave Symposium (IMS)*, 2016 IEEE MTT-S International. IEEE, 2016.

[3] Wu, Qianteng, et al. "Frequency translational RF receiver with time varying transmission lines (TVTL)." *Microwave Symposium (IMS),* 2017 IEEE MTT-S International. IEEE, 2017.

[4] Biedka, Mathew M., et al. "Ultra-wide band non-reciprocity through sequentially-switched delay lines." *Scientific reports* 7 (2017): 40014.

[5] Yu, Zongfu, and Shanhui Fan. "Complete optical isolation created by indirect interband photonic transitions." *Nature photonics* 3.2 (2009): 91.

[6] Fleury, Romain, et al. "Sound isolation and giant linear nonreciprocity in a compact acoustic circulator." *Science* 343.6170 (2014): 516-519.

[7] Chao, G. "Parametric amplification of surface acoustic waves." *Applied Physics Letters* 16.10 (1970): 399-401.

[8] Inaba, R., and N. Mikoshiba. "Parametric amplification of surface acoustic wave of ZnO-Ga-doped yttrium iron garnet." *Applied Physics Letters* 41.1 (1982): 25-26.

[9] Rotter, M., W. Ruile, and A. Wixforth. "Non-reciprocal SAW devices for RF applications." *Ultrasonics Symposium*, 2000 IEEE. Vol. 1. IEEE, 2000.

[10] Basceri, Cem, et al. "The dielectric response as a function of temperature and film thickness of fiber-textured (Ba, Sr) TiO 3 thin films grown by chemical vapor deposition." Journal of Applied Physics 82.5 (1997): 2497-2504.

[11] Noeth, Andreas, et al. "Tunable thin film bulk acoustic wave resonator based on Ba x Sr 1-x TiO 3 thin film." *IEEE transactions on ultrasonics, ferroelectrics, and frequency control* 57.2

(2010).

[12] Gevorgian, Spartak, Alexander Tagantsev, and Andrei K. Vorobiev. "Tuneable film bulk acoustic wave resonators. " *Springer Science & Business Media*, 2013.

[13] Smith, W. Richard, et al. "Analysis of interdigital surface wave transducers by use of an equivalent circuit model." *IEEE Transactions on Microwave Theory and Techniques* 17.11 (1969): 856-864.

[14] Pozar, David M. "Microwave engineering. " *Publishing House of Electronics Industry*, 2006.